HAL
open science

Mechanisms for picrotoxin block of alpha2 homomeric glycine receptors.

D.S. Wang, J.M. Mangin, G. Moonen, J.M. Rigo, P. Legendre

To cite this version:

D.S. Wang, J.M. Mangin, G. Moonen, J.M. Rigo, P. Legendre. Mechanisms for picrotoxin block of alpha2 homomeric glycine receptors.. Journal of Biological Chemistry, 2005, 281, pp.3841-3855. 10.1074/jbc.M511022200 . hal-00086049

HAL Id: hal-00086049

https://hal.science/hal-00086049

Submitted on 17 Jul 2006

HAL is a multi-disciplinary open access archive for the deposit and dissemination of scientific research documents, whether they are published or not. The documents may come from teaching and research institutions in France or abroad, or from public or private research centers.

L'archive ouverte pluridisciplinaire **HAL**, est destinée au dépôt et à la diffusion de documents scientifiques de niveau recherche, publiés ou non, émanant des établissements d'enseignement et de recherche français ou étrangers, des laboratoires publics ou privés.

Cet article a été publié dans J Biol Chem. (2006) 281, 3841-3855

MECHANISMS FOR PICROTOXIN BLOCK OF α_2 HOMOMERIC GLYCINE RECEPTORS

Dian-Shi Wang[1,4], Jean-Marie Mangin[2], Gustave Moonen[2], Jean-Michel Rigo[2,3], and Pascal Legendre[1]

[1] UMR CNRS 7102 Neurobiologie des Processus Adaptatifs, Université Pierre et Marie Curie, 9 quai St Bernard, 75252, Paris cedex 05, France.

[2] Centre de Recherche en Neurobiologie Cellulaire et Moléculaire, Faculté de Médecine de Liège, 17 place Delcour, B-4020 Liège 2, Belgique.

[3] Universiteit Hasselt, Biomed Research Center, Agoralaan, B-3590 Diepenbeek, België.

[4] Department of Anatomy, Fourth Military Medical University, Xi'an 710032, China..

Running title: PTX inhibition of α_2 homomeric GlyR

Address correspondence: Dr. Pascal Legendre, UMR CNRS 7102 Neurobiologie des Processus Adaptatifs, Université Pierre et Marie Curie, case 1, 9 quai St Bernard, 75252 Paris cedex 05, France. Tel: + 1 44 27 25 19; Fax: + 1 44 27 27 81.

Email: pascal.legendre@snv.jussieu.fr

It is well known that the convulsant alkaloid picrotoxin (PTX) can inhibit neuronal GABA and homomeric glycine receptors (GlyR). However, the mechanism for PTX block of α_2 homomeric GlyR is still unclear compared to that of α_1 homomeric GlyR, $GABA_A$ and $GABA_C$ receptors. Furthermore, PTX effects on GlyR kinetics have been poorly explored at the single-channel level. Hence, we used the patch-clamp technique in the outside-out configuration to investigate the mechanism of PTX suppression of currents carried by α_2 homomeric GlyRs stably transfected into Chinese hamster ovary cells. PTX inhibited the α_2 homomeric GlyR current elicited by glycine in a concentration-dependent and voltage-independent manner. Both competitive and noncompetitive mechanisms were observed. PTX decreased the mean open time of the GlyR channel in a concentration-dependent manner, suggesting that PTX can block channel openings and bind to the receptor in the open channel conformation. When PTX and glycine were co-applied, a small rebound current was observed during drug washout. Application of PTX during the deactivation phase of glycine-induced currents eliminated the rebound current and accelerated the deactivation time-course in a concentration-dependent manner. PTX could not bind to the unbound conformation of GlyR, but could be trapped at its binding site when the channel closed during glycine dissociation. Based on these observations, we propose a kinetic Markov model in which PTX binds to the α_2 homomeric GlyR in both the open channel state and the fully-liganded closed state. Our data suggest a new allosteric mechanism for PTX inhibition of wild-type homomeric α_2 GlyR.

Glycine and GABA are the main inhibitory neurotransmitters in the central nervous system. The glycine receptor (GlyR) is a pentameric transmembrane protein complex, which forms an anion-selective channel (1). Five different subunits have hitherto been cloned in mammals, one α subunit and four β subunits (β_1-β_4) which are associated with two different ways of forming functional receptors: the homomeric configuration composed of five α subunits (1) and the heteromeric configuration comprising two α subunits and three β subunits (2). In the adult brain, GlyR is primarily involved in fast inhibitory synaptic transmission in the brainstem and spinal cord.

It is now well established that picrotoxin (PTX), a plant alkaloid, which was first used to discriminate GABAergic from glycinergic currents, can also strongly inhibit the homomeric GlyR subtypes, whereas the α/β heteromeric GlyR subtype is much less sensitive to PTX (3). Although the action of PTX has been extensively studied both on $GABA_A$, and $GABA_C$ receptors and on GlyRs (4), the binding site(s) of this compound and its inhibitory mechanism are still under debate. There are lines of evidence indicating that PTX binding and/or inhibitory mechanisms are related to amino acid residues in the transmembrane domain TM2 forming the pore of the ionic channel (3, 5-13). A series of studies on the $GABA_AR$, $GABA_CR$, invertebrate glutamate receptor Cl^- channel (GluClR) and GlyRs has established that a ring of 6' threonines within the pore is invariably required for PTX sensitivity (4). Recently, it has been accurately demonstrated that PTX is likely to bind in the channel pore of the homomeric α_1 GlyR (14). Although PTX could be trapped when the GlyR channel closed in the α_1 subunit R271C mutation, this was not the case for wild-type GlyR (14) and it is unlikely that PTX can act as an open channel blocker on this GlyR subtype. In fact, the inhibitory mechanism of PTX can differ between anionic receptor-channel family subtypes and it ranges from open channel blocker to allosteric competitive antagonist (4). Although in some preparations PTX inhibition of $GABA_AR$ appeared to be use-dependent and noncompetitive (15), suggesting an open channel

block mechanism for PTX inhibition, analysis of PTX-evoked inhibition of the single-channel activity of $GABA_AR$ recorded from rat sympathetic neurons indicates that PTX inhibition is not use-dependent (16). In this study, the authors proposed that PTX preferentially binds to the agonist-bound conformation of the receptor and stabilized the channel in the closed state (16). This was also demonstrated with $GABA_C$ receptors from isolated retinal bipolar cells and from oocytes expressing the GABAR ρ subunit (17). A competitive inhibitory component of PTX inhibition has been described for homomeric α_1 GlyR. Its potency decreased as agonist concentration increased (18). But PTX is unlikely to modify glycine binding and it was proposed that PTX rather acts as an allosteric inhibitor by altering the coupling between agonist binding and channel gating (18). Although extensive efforts have been made to determine the molecular mechanism of PTX inhibition of GlyRs, paradoxically little work has been done on the single-channel effects of PTX on GlyR kinetics. It has only been shown that at low concentrations (1-30 μM) PTX decreased the probability of predominantly high conductance with homomeric α_1 GlyRs. In contrast, at higher concentrations PTX induced flickering closures in both heteromeric α_1/β GlyRs and homomeric α_1 GlyRs (19, 20).

The α_2 homomeric GlyR subunit has been identified as an embryonic receptor form (21, 22) and plays an important role during synaptogenesis and cell differentiation. It is more adapted to sustained and slow paracrine neurotransmitter release (23) as observed in the fetal brain (24). It has recently been shown that PTX is as potent on homomeric α_2 GlyRs (25) as on homomeric α_1 GlyRs (3, 18, 19). Furthermore, α_2 homomeric GlyR has slow kinetic properties (23) and opens mainly with a single large conductance state (100-120 pS), which makes this receptor a good model for analyzing the effect of PTX on GlyR kinetics.

Therefore, we investigated here the mechanism of inhibition of PTX on the activation and deactivation kinetics of the homomeric α_2 GlyR expressed in Chinese hamster ovary (CHO) cells as a model system, by means of outside-out patch clamp recordings using an ultra-fast flow application system. We showed that PTX inhibited α_2 homomeric GlyRs in a concentration-dependent and voltage-independent manner, and that PTX could bind to the receptor in both the open channel conformation and the fully-liganded closed state. We also demonstrated that PTX could be trapped at its binding site when the channel closed during glycine dissociation. This complex mechanism can be predicted by a simple kinetic model in which glycine can dissociate while PTX remains bound.

Materials and Methods

Cell culture - Chinese hamster ovary cells (CHO-K1, ATCC no. CCL61) were maintained in a 95% air-5% CO_2 humidified incubator at 35°C in Dulbecco's modified Eagle's medium (DMEM) supplemented with 0.11 g/L sodium pyruvate, 6 g/L D-glucose, 10% (v/v) heat-inactivated fetal bovine serum (all from GIBCO BRL). Cells were passaged every 5-6 days (up to 20 times). For electrophysiological recordings, cells were seeded onto glass coverslips coated with poly-L-ornithine (0.1 mg/ml). Glycine receptor α_2 subunit cloning and transfection were performed as previously described (23).

Outside-out recordings - Outside-out recordings (26) were done under direct visualization on α_2 GlyR transfected CHO cells with the use of Normaski optics (X 40; immersion lens; Nikon Optiphot). Cells were continuously perfused at room temperature (20-22°C) with oxygenated bathing solution (2 mL/min) containing (in mM): NaCl 147, KCl 2.4, $CaCl_2$ 2, $MgCl_2$ 2, HEPES 10, Glucose 10 (pH 7.2, osmolarity 320 mOsm). Patch-clamp electrodes (5-10 MΩ) were pulled from thick-wall borosilicate glass with an outer diameter of 1.5 mm and inner diameter of 0.86 mm (Harvard Apparatus, Kent, UK) in multiple steps using a Brown-Flaming puller (Sutter Instrument Co., Navato, USA). They were fire-polished and filled with (in mM): CsCl 130, $MgCl_2$ 4, Na_2ATP 4, EGTA 10, HEPES 10 (pH 7.2, osmolarity 290 mOsm). Currents were recorded using an Axopatch 1D amplifier (Axon Instruments, Foster City, USA), and stored using a digital recorder (PCM-R300, Sony, Tokyo, Japan). Recordings were filtered at 10 kHz using an eight-pole bessel filter (Frequency Devices, Haverhill, USA), sampled at 50 kHz and stored on a PC computer using pClamp software 6.03 (Axon Instruments, Foster City, USA). The membrane potential was held at -50 mV throughout the experiment, except when examining the *I-V* relationship. Patch currents represent the average of 10 or more trials as specified in the figure legends or the text unless otherwise noted.

Drug delivery - Outside-out single-channel currents were evoked using a fast-flow operating system (27, 28). Control and drug solution were gravity-fed into two channels of a thin-wall glass theta tube (2 mm outer diameter; Hilgenberg, Malsfeld, Germany) pulled and broken to obtain a 200 μm tip diameter. The outside-out patch was positioned (45° angle) 100 μm away from the theta tubing, to be close to the interface formed between the flowing control and drug solutions. One lumen of the theta tube was connected to reservoirs filled with solutions containing glycine and/or PTX. The solution exchange was performed by rapidly moving the

solution interface across the tip of the patch pipette, using a piezo-electric translator (model P245.30, Physik Instrument, Waldbronn, Germany). Concentration steps of glycine lasting 1-1000 ms were applied with an interval of ≥ 10 s. Exchange time of 10-90% (< 100 μs) was determined before each set of experiments by monitoring the change in the liquid junction potential evoked by the application of a 10%-diluted control solution to the open tip of the patch pipette (28). For the experiments requiring fast solution exchange between three different conditions (see figure 8), we used a homemade multi-barrelled application system composed of three horizontally aligned quartz tubes (inside diameter 0.25 mm; outside diameter 0.35 mm; Polymicro Technologies). Solution exchange was achieved by lateral movements, using a SF-77B fast-step perfusion system (Warner Instruments, Hamdell, CT, USA). The complete solution change was achieved in 200-300 μs. Glycine and PTX were from Sigma (St Louis, USA). Stock solution of PTX was prepared in dimethyl sulfoxide (DMSO) and then diluted to an appropriate concentration with the above extracellular solution just before use. The final concentration (v/v) of DMSO was not higher than 0.3%, which had no effect on α_2 homomeric GlyRs as verified by control experiments (data not shown).

Data analysis - Outside-out currents were analyzed off-line on a G4 Macintosh using Axograph 4.9 software (Axon Instruments, Foster City, USA). The concentration–inhibition curve of PTX was fitted using the Hill equation:

$$\frac{I}{I_{\mathrm{Con}}} = \frac{1}{1 + \left[\frac{[PTX]}{IC_{50}}\right]^{n_H}}$$

where I is the response in the presence of PTX, I_{Con} is the control response (i.e. the glycine response in the absence of PTX), IC_{50} is the PTX concentration at which half of the glycine response is blocked, and n_H is the Hill coefficient. For each concentration tested, the amplitude of the current, I, was measured at the steady-state level. The activation time constants of glycine-evoked currents in the presence and absence of PTX were estimated by fitting the onset of the responses with a sum of exponential curves using Axograph 4.9 software. Decay time constants were obtained by fitting the first 750 ms of the decay phase with a sum of exponential curves using Axograph 4.9 software (Axon Instruments, USA). The presence of one or more exponential components was tested by comparing the sum of squared errors of the fits (28, 29).

For single-channel analysis, patches with one channel were included only if channel activity was stable over sweeps. First latencies, open and closed time durations were measured manually using Axograph 4.9 software. First latency distributions were created using standard histogram techniques (30). For display purposes, open and closed time histograms show the distributions as log intervals with the ordinate on a square root scale. These distributions were fitted with the sum of several exponential curves. The fit was optimized with the least square method (31). The number of exponential components was determined by comparing the sum of squared errors of the fits.

Kinetic modeling programs - To obtain a kinetic model for PTX effects on GlyR behavior, glycine-evoked currents in the absence and presence of PTX were analyzed off-line, and the inhibitory effect of PTX on GlyR kinetics was mathematically modeled using the chemical kinetic modeling programs included in the Axograph 4.9 software package (Axon Instruments, USA). This program first calculated the change in the number of channels in each given state for given rate constants, and then systematically varied the rate constants to give the minimum sum of squared errors (SSEs) between the experimental data and a given model transient (29). Outside-out responses from 12 patches evoked by the application of glycine in the absence or presence of PTX were used for kinetic modeling analysis. Models were compared using the resulting SSE values of the fit.

Averaged data are expressed as mean ± S.E.M., except when stated otherwise. Statistical significance of the data was assessed by means of Student's *t* test or one-way analysis of variance (ANOVA) followed by Dunnett's multiple-comparison post tests when significance was reached.

Results

Concentration-dependent inhibition of α_2 homomeric GlyR by PTX

We first analyzed the ability of PTX to inhibit GlyR activity in terms of the outside-out current evoked by glycine applications to patches containing recombinant α_2 homomeric GlyR from CHO cells stably expressing the α_2 GlyR subunit. Figure 1A illustrates the inhibitory effect of different concentrations of PTX on inward currents (V_H = -50 mV) evoked by 300 μM glycine (left traces; near the EC_{50} for glycine-evoked response, see 23) and 30 mM glycine (right traces). In these experiments glycine was coapplied with PTX at concentrations indicated by the number below each trace. The co-application of PTX and glycine caused a concentration-dependent reduction of the current amplitude. The effect of PTX was reversible after washout. Interestingly, after co-application of 10 μM PTX and 300 μM glycine, when the two compounds were simultaneously withdrawn, a small transient membrane current was observed before current relaxation (figures 1A, 2A). Figure 1B shows the concentration-response curves for PTX coapplied with two different concentrations of glycine obtained in twelve outside-out experiments. Concentration-response curves were fitted with the Hill equation (see Materials and Methods) and in the presence of 300 μM glycine gave an IC_{50} (half-maximum inhibition) and a Hill coefficient of 2.7 ± 0.2 μM and 0.8 ± 0.04, respectively. When glycine concentration was increased to 30 mM, the concentration-response curve was shifted to the right and the IC_{50} value increased to 6.4 μM. The Hill coefficient value was not modified (0.8 in the presence of 30 mM glycine). This glycine concentration-dependent shift in PTX IC_{50} was previously described for α_1 homomeric GlyRs and was thought to reflect a competitive inhibitory mechanism (18). However, it should be noted that PTX is unlikely to be a true competitive antagonist, since increasing the glycine concentration from 30 mM to 100 mM only slightly reduced the inhibitory effect of 10 μM PTX. The percentage inhibition of PTX-evoked outside-out current was 57 ± 2% (n = 12) and 50 ± 3% (n = 8) in the presence of 30 mM glycine and of 100 mM glycine, respectively.

PTX-induced inhibition is not voltage-dependent

The small rebound current observed during GlyR deactivation immediately after the termination of co-application of 10 μM PTX and glycine (figures 1A, 2A) could reflect the recovery from PTX open channel block as described for the open-channel block effect of acetylcholine on nicotinic receptors (32, 33). If PTX acts as a classic fast open channel blocker, the inhibitory effect of this alkaloid must be voltage-dependent. To test this hypothesis, the voltage dependence of PTX-induced glycine current inhibition was examined. Typical examples of 300 μM glycine-evoked currents (1s application step) at V_H of + 50 and - 50 mV with and without co-application of 10 μM PTX are shown in figure 2*A*. In this example PTX inhibited glycine-evoked currents both at positive and at negative holding potentials. Voltage dependence of PTX inhibition on glycine-evoked currents was analyzed by constructing *I-V* curves from 300 μM glycine-evoked currents in the absence and presence of 10 μM PTX at holding potentials ranging from –70 mV to + 70 mV (figure 2B). As shown in figure 2B, the steady-state current of the responses evoked in the absence or presence of PTX varied linearly at negative potentials and rectified at positive potentials. Adding PTX to glycine solution did not significantly change the reversal potential (*V*r) of the glycine-evoked currents (unpaired *t*-test, $P > 0.1$). *V*r was − 3 mV with glycine and − 4 mV with glycine + PTX. The voltage-independent nature of PTX block was revealed by plotting the percentage of block evoked by co-application of 10 μM PTX and 300 μM glycine at holding potentials ranging from + 70 mV to - 70 mV (figure 2C). Over this potential range PTX reduced the amplitude of glycine currents to the same extent (−70%), indicating that PTX might not bind to a site within the membrane field of α_2 homomeric GlyRs. Nevertheless, PTX is weakly charged at neutral pH and the lack of a voltage-dependent block does not exclude the possibility that PTX can bind within the channel pore as recently suggested (14).

PTX accelerates the deactivation kinetics of glycine-evoked current.

A previous study has shown that PTX applied immediately after GABA accelerates the deactivation kinetics of $GABA_CR$ (17). To determine if PTX has any effect on GlyR deactivation kinetics, we first compared the deactivation phase of the outside-out currents evoked by co-application of glycine and PTX or in the continuous presence of PTX before, during and after glycine application (figure 3A). When compared to responses evoked by simultaneous application of 300 μM glycine and 10 μM PTX, the continuous presence of PTX dramatically accelerated the deactivation time-course of the responses. In control conditions and after co-application of glycine and PTX the deactivation time constant (τ_{decay}) was 135 ± 9 ms (*n* = 13) and 133 ± 7 ms (*n* = 13), respectively. During the continuous presence of 10 μM PTX, the deactivation time constant was significantly decreased to 30 ± 3 ms (*n* = 13) (paired *t*-test $P < 0.01$). Continuous application of PTX also accelerated the deactivation phase of responses evoked by a short (1 ms) step of a saturating concentration of glycine (30 mM, figure 3B1). As the PTX concentration increased, the deactivation time constants decreased in a concentration-dependent manner (figure 3B2). The decay phase of outside-out currents evoked by 1 ms application of 30 mM glycine was well fitted with a single exponential

function, giving a τ_{decay} of 117 ± 12 ms (n = 10). In the presence of continuous PTX, τ_{decay} significantly decreased to 67 ± 2 ms for 1 μM PTX (n = 7), 45 ± 3 ms for 3 μM PTX (n = 10), 31 ± 4 ms for 10 μM PTX (n = 6) and 15 ± 2 ms for 30 μM PTX (n = 5), respectively (ANOVA; $P < 0.01$).

The deactivation phase of the responses evoked by a short concentration pulse of agonist reflects channel reopening before the agonist can dissociate from its binding sites. In a simple kinetic model with several liganded closed states and in the absence of any open channel blocker or inhibitory drugs promoting closed states from the open state, the deactivation time constant is a good approximation to the mean burst duration. This is the case for homomeric α_2 GlyRs (23). For homomeric α_2 GlyRs the mean burst duration during deactivation depends on the mean open time of the channel, the mean closed time, the number of openings and the number of closures. The mean burst duration τ_b = No/α + Nc/(α+k_{off}), where α is the opening rate constant, β the closing rate constant, k_{off}, the dissociation rate constant for glycine, No the number of openings per burst (No = 1+α/k_{off},) and Nc the number of closures per burst (Nc = β/k_{off},) (34). In the case of a simple fast open channel block mechanism with no other way than the open state for the channel to escape from the block, the mean open time of each opening within a burst must decrease but the mean burst length must be increased, which slows down the relaxation (34). In contrast, slow blockers must shorten the openings on average and limit reopening of the channel during relaxation. Such slow blockers will appear to speed up relaxation. Besides these two extreme blockers, an intermediate blocker must evoke a biphasic relaxation (34). In our experiments, PTX decreased in a concentration-dependent manner the deactivation time constant of the current evoked by a short concentration step of glycine (figure 3B). In this case the relaxation can still be fitted by a single exponential curve, which favors the hypothesis of slow blocker-like mechanisms for PTX. If so, PTX must also decrease the mean open time of the channel to the same extent as the deactivation time constant of the glycine-evoked currents.

To determine the microscopic determinants of the decrease in the decay time constant, we have analyzed the open time and closed time distributions in single receptor burst of openings in response to short (1 ms) concentration pulses of glycine near GlyR saturation (30 mM) in the absence and presence of PTX. To perform this analysis, patches with a single functional GlyR were selected (i.e. patches that did not display superimposed openings in response to a saturating concentration of agonist; see 23). Single openings and closures were manually detected and measured using a filter cut-off frequency of 5 kHz. In control conditions, GlyR opens in bursts of long openings interrupted by very short closures (figure 4A). In the presence of continuous 10 μM PTX, the single opening duration appeared to be shortened (figure 4B). Opening and closing time constants were estimated by pooling measurements made on these single-channel responses obtained from 7-9 patches (23). The open time histograms were best fitted by single exponential curves both in control conditions and in the presence of continuous PTX (figures 4C,D). In control conditions, the mean open time was 48.4 ms which is consistent with the value we obtained previously (23). The mean open time was decreased to 6.1 ms in the presence of 10 μM PTX. In control conditions, the closed time distribution was best fitted by a single exponential curve with a closed time constant τ_c = 0.27 ms, as previously described for homomeric α_2 GlyRs (23). In the presence of PTX (10 μM) the closed time distribution was best fitted by the sum of 2 exponential curves giving a τ_{c1} = 0.23 ms, which is very similar to the closed time constant in the control conditions. A second closed time was detected in the presence of PTX with a time constant τ_{c2} = 5.76 ms (figure 4F). This longer closed time is likely to reflect an additional recovery pathway from PTX-evoked open channel block.

The ensemble-averaged currents obtained by averaging single channel responses (116 trials for 30 mM glycine, 202 trials for continuous 10 μM PTX) indicated a τ_{decay} similar to that observed for macroscopic glycine currents in the absence and presence of continuous PTX (figure 3). τ_{decay} was 131 ms and 31 ms, respectively for the averaged currents in the absence and presence of continuous PTX (figures 4 A, B bottom). Altogether these results indicate that the decrease in the deactivation time constant evoked by PTX could be mainly due to a decrease in the mean open time of the channel. If this hypothesis is true, increasing PTX concentration must decrease the mean open time in a concentration-dependent manner as it does for the deactivation time constant of the glycine-evoked current (see figure 3B).

To obtain more precise information on the block mechanism of PTX, we analyzed the effect of increasing PTX concentration on the mean open time of the GlyR channel. Such analysis will also give us information on the blocking rate constant of PTX (34). We analyzed the open time distributions in single receptor bursts of openings in response to 30 mM concentration pulses (200 ms) of glycine (see figures 7A, B). Opening time constants were analyzed by pooling measurements made on 22-66 sweeps from 1-3 patches. Histograms of the open durations within bursts in the absence and presence of PTX were constructed and were best fitted by single exponential curves at all PTX concentrations tested (figures 5A-C). As expected, PTX decreased the mean open time in a concentration-dependent manner. The mean open time for the control response was 50.1 ms (66 trials from 3 patches; figure 5*A*). In the presence of continuous PTX, the mean open time decreased to 26.2, 16.2, 6.3 ms and 2.7 ms, for 1 μM PTX (44

trials from 3 patches), 3 μM PTX (52 trials from 3 patches), 10 μM PTX (47 trials from 3 patches), and 30 μM PTX (22 trials from 1 patch), respectively (figures 5*B-D*). These results indicate that PTX inhibition can be related to an open channel blocker mechanism (34).

To obtain an approximation of the binding rate constant for PTX, the reciprocals of the mean open times were plotted as a function of the PTX concentration as shown in figure 5D. Binding (k_{on}) and closing (β) rate constants were calculated from the relationship $1/\tau_o = [PTX]k_{on} + \beta$ (34), where τ_o is the mean open time and [PTX] is the PTX concentration. The linear fit to the data gave k_{on} = 11.6 $\mu M^{-1}s^{-1}$ and an β value of 27.9 s^{-1}.

PTX slows down the activation kinetics of glycine-evoked current

The activation phase of current evoked by concentration steps of agonist gives important information on the kinetics of the receptor channels (23). The effects of PTX on the rising phase of macroscopic averaged currents evoked by glycine on α_2 homomeric GlyRs were therefore analyzed (figure 6). A series of 10-25 trials evoked with ≥ 10 s intervals was used to generate macroscopic currents as shown in figure 6A. The duration of the applications was adjusted to obtain a steady-state current. The rising phases of the outside-out currents evoked by the application of 300 μM glycine were best fitted with the sum of two exponential curves giving a fast rising time constant (τ_{fast}) and a slow rising time constant (τ_{slow}) as previously described (23). As shown in figure 6B, there was no significant difference in the τ_{fast} of currents activated by 300 μM glycine alone (τ_{fast} = 38 ± 5 ms, *n* = 14), during co-applications of glycine and PTX (τ_{fast} = 24 ± 5 ms *n* = 13) or during the continuous application of PTX, before, during and after glycine application (τ_{fast} = 24 ± 4 ms *n* = 12) (ANOVA, $P > 0.05$). τ_{slow} in the presence of co-application of 10 μM PTX and 300 μM glycine was significantly decreased, compared to responses evoked by glycine application alone (paired *t*-test, $P < 0.05$). These results could suggest that PTX had little or no effect on glycine binding.

For homomeric α_2 GlyRs, $\tau_{fast} = 1/(\beta+\alpha([glycine]^n/([glycine]^n+rEC_{50}^n)))$ where [glycine] is the concentration of the agonist, n the hill coefficient and rEC_{50} is the concentration of glycine that gives half of the maximum opening rate constant α (23). Therefore, in order to determine whether the opening rate constant α was modified by PTX or not, we analyzed the rising phase of the currents evoked by a saturating concentration of glycine (30-100 mM) in the absence and presence of PTX. For such saturating concentrations, the faster rising time constant $\tau_{fast} \approx 1/(\beta+\alpha)$ and is moreover mainly controlled by β since α is > 200 times faster than β for homomeric α_2 GlyRs (23). Measurements were performed on averaged traces of 12-25 trails. In control conditions the rising phase of the currents evoked by 30 mM glycine was well fitted with the sum of two exponential curves in 12 out of 17 patches (figures 6C,D) with time constants τ_{fast} = 0.27 ± 0.03 ms and τ_{slow} = 3.1 ± 0.5 ms (*n* = 12). As shown in figures 6E and F, simultaneous application of 30 mM glycine and 10 μM PTX did not significantly change the rising time constants as expected if the α value was not modified by PTX applications (paired *t*-test $P > 0.1$). In the presence of PTX, τ_{fast} = 0.26 ± 0.03 ms and τ_{slow} = 2.6 ± 0.8 ms (n = 12). Surprisingly, when 10 μM PTX was continuously applied before, during and after 30 mM glycine successive concentration steps (application frequency 0.1Hz), the rising phase of the first glycine-evoked response was unchanged while it was slowed down for the next responses (data not shown). This PTX effect on the rising phase of glycine-evoked responses was analyzed on averaged traces (12-15 sweeps; figure 6C). In this case both τ_{fast} and τ_{slow} were significantly increased (paired *t*-test, $P < 0.01$). During continuous application of 10 μM PTX, τ_{fast} = 2.1 ± 0.4 ms and τ_{slow} = 15.2 ± 3.0 ms (*n* = 12). Increasing the glycine concentration to 100 mM (figure 6D) did not prevent this PTX effect, confirming that it cannot result from modifications in glycine binding kinetics (figures 6E,F). In control conditions, the rising phase of the responses evoked by the 100 mM concentration step of glycine was well fitted by two exponential curves in 8 out of 11 patches tested (in the other patches the rising phase was fitted with a single exponential function; see 23). In this case, τ_{fast} = 0.26 ± 0.03 ms and τ_{slow} = 3.1 ± 0.6 ms (*n* = 8). With continuous application of PTX, τ_{fast} and τ_{slow} increased to 2.1 ± 0.3 ms and 15.0 ± 2.5 ms, respectively (*n* = 8). This was not significantly different from the measurements obtained with 30 mM glycine (unpaired *t*-test, $P > 0.1$)

An increase in the first latency accounts for the increase in the two activation time constants.

To determine if the increase in the two activation time constants of the rising phase of the currents that we observed in the presence of continuous application of PTX reflects changes in GlyR behavior occurring before channel conformational changes leading to the open state, we analyzed the distribution of initial closed times leading to the first opening (first latencies) in outside-out patches containing one active GlyR (see Materials and Methods). Figures 7A and B show the activation of a single receptor from the same patch in response to 200 ms step applications of 30 mM glycine in the absence (figure 7A) or in the continuous presence (figure 7B) of 10 μM PTX (application frequency 0.1 Hz). The ensemble-averaged current obtained by averaging single channel responses (229-266 trials) had time-courses similar to those observed for macroscopic currents in the absence or presence of continuous application of

PTX, as previously described (see figure 6). As shown for macroscopic currents, the ensemble-averaged currents also exhibit a biphasic rising phase with fast and slow components, which were considerably slowed down in the continuous presence of PTX. The increase in the activation time constants observed in the presence of PTX appeared to be related to an increase in the first latency (FL) duration. The FL cumulative distributions of the activation of a single GlyR evoked by 30 mM glycine application in the absence or presence of 10 μM PTX are shown in figures 7C,D. The FL distributions were best fitted by the sum of two exponential functions with time constants τ_{fast} = 0.24 ms (85%), τ_{slow} = 2.2 ms (15%) in the absence of PTX and τ_{fast} = 4.7 ms (61%), τ_{slow} = 18.9 ms (39%) in the presence of continuous PTX. The corresponding ensemble-averaged current exhibited a rising phase with τ_{fast} = 0.33 ms (90%), τ_{slow} = 2.4 ms (10%) in the absence of PTX and τ_{fast} = 5.1 ms (48%), τ_{slow} = 20.7 ms (52%) in the presence of PTX, indicating that the slower activation phase of the ensemble current in the presence of continuous PTX was related to changes in GlyR conformational closed states distal from the channel open state.

Recovery from PTX block requires channel reopening

A lengthening in the rise time of responses evoked by PTX pre-incubation has been described for GABA-evoked outside-out currents in crayfish muscle (35). This was interpreted as the consequence of PTX binding to the unliganded receptor (35). To test this hypothesis on GlyRs, we analyzed the effects of PTX pre-treatment on current evoked by the application of 10 mM glycine alone. Since the lengthening in the current rising phase observed for GABA-evoked outside-out current is likely to reflect recovery from PTX inhibition in the presence of the agonist alone (35), we first estimated for comparison the recovery time constant of PTX inhibition by a transient application of 10 μM PTX during glycine-evoked currents. As shown in figure 8A, transient application of PTX evoked a fast decrease in glycine current with a time constant of 17.0 ± 2.6 ms (n = 7) (figure 8A). At the end of the application of PTX, current amplitude increased progressively. This recovery phase from PTX inhibition was best fitted by a bi-exponential curve with time constants τ_{fast} = 2.6 ± 0.4 ms (20 ± 2 %) and τ_{slow} = 21.7 ± 3.9 ms (80 ± 2 %) (n = 7)..

When 10 μM PTX was applied immediately before (time interval < 0.1 ms) a concentration step of a saturating concentration of glycine (10 mM), it did not change the amplitude of the glycine-evoked current or its rising phase (figure 8B). The activation time constants were τ_{fast} = 0.4 ± 0.04 ms (81 ± 5%) and τ_{slow} = 2.6 ± 0.7 ms (19 ± 5%) ms in control conditions, and τ_{fast} = 0.4 ± 0.04 ms (82 ± 9%) and τ_{slow} = 2.4 ± 0.2 ms (18 ± 9%) ms with PTX pre-treatment (n = 5). This was not significantly different (paired t-test, $P > 0.5$). These data indicate that it is unlikely that PTX can bind to unliganded GlyR.

According to the results described above, the lengthening of the rise time we observed in the continuous presence of PTX is unlikely to be due to PTX binding to unliganded GlyR. Moreover, simultaneous application of PTX and glycine had no significant effect on the rise time of the outside-out current. The only possibility of the lengthening of the rise time we observed in the continuous presence of PTX is that PTX, when applied during the deactivation of the glycine-evoked currents, modifies the activation kinetics of the next response. This hypothesis implies that PTX preferentially binds to GlyR in the open state and that it can remain bound after glycine washout. A similar PTX inhibitory effect was recently described for mutated R271C homomeric α_1 GlyRs (14). To test this hypothesis we analyzed the effect of PTX on the rise time of successive responses evoked by glycine when this alkaloid was applied during the relaxation phase of the first response (PTX post-treatment). PTX was applied for 500 ms, which corresponds to the full time-course of the deactivation phase of the glycine-evoked current without PTX. For these experiments we selected patches with a large number of GlyRs. This allowed us to compare the rise time between individual traces. The activation time constants were measured for glycine responses evoked 60 s after PTX post-treatment. They were compared with the values obtained in control conditions. To determine if this effect of PTX was reversible, we analyzed the rise time of responses evoked 3 s after the second application of glycine alone. As shown in figure 8C, post-treatment with 10 μM PTX was sufficient to speed up the deactivation phase of glycine-evoked current. The current evoked by the application of glycine alone up to 60 s after the end of the glycine current plus PTX post-treatment had an amplitude similar to that of the control response (< 5% decrease; n = 7). Surprisingly, this current had a significantly slower rise time than that of control (n = 7, paired t-test, $P < 0.01$). This was due to slower rising time constants τ_{fast} and τ_{slow} and to an increase in the proportion of the slow component of the activation phase. The activation time-course of these responses was well fitted by the sum of two exponential curves as in the control, but with time constants τ_{fast} = 2.2 ± 0.2 ms (38 ± 1%) and τ_{slow} = 31 ± 3 ms (62 ± 1%). Applying glycine after (3 s) the response with a slower rising phase (figure 8C) evoked a current with activation time constants very similar to control values: τ_{fast} = 0.5 ± 0.04 ms (85 ± 5%) and τ_{slow} = 3.1 ± 0.3 ms (15 ± 5%). These results clearly indicate that the lengthening of the rise time evoked by PTX can persist up to 60 s after washout of glycine and PTX. They also indicate that GlyRs must be reactivated to allow recovery from the PTX effect. It is therefore likely that PTX can be trapped at its binding site when

the channel closes and/or when glycine molecules dissociate from their binding sites.

A minimal Markov model for PTX inhibition

To account for the data obtained on PTX inhibition of homomeric α_2 GlyR, we adopted the minimal Markov model previously proposed for this GlyR subtype (23). This model has two binding sites for glycine, two desensitization closed states and a single open state linked to the doubly liganded closed state. Each desensitization state is linked to the mono-liganded closed state and the doubly liganded closed state, respectively. But this model has some limitations since it has a tendency to underestimate the time constant values of the rising phase of the currents evoked by glycine concentrations lower than the EC_{50} of glycine (23). We overcame this problem by adding a third binding site linked to another desensitization state (figure 9A), as recently proposed for homomeric α_1 GlyR (36). Before testing the Markov models accounting for PTX inhibition, we first adjusted the different rate constants of the model describing glycine-elicited responses for each control trace. To do so we fitted experimental traces obtained by a long application of 0.3 and 30 mM glycine (23, 37). The average kinetic parameters derived from model fitting of glycine-evoked outside-out currents are listed in Table 1. This model predicts a glycine EC_{50} of 240 μM and a Hill coefficient of 2, which are in good agreement with previously published values (200 μM and 1.9, respectively) (23).

Having established the kinetic parameters for glycine-evoked currents, we then analyzed PTX inhibition responses on the same traces. The kinetic model for PTX inhibition was elaborated according to our experimental data. According to the Hill coefficient (≈ 1) of the concentration-response curve for PTX, we first postulated that only one PTX molecule binds to GlyR. This is consistent with what is known about PTX inhibition of $GABA_C$ receptors (17), crayfish muscle GABA receptors (35) and homomeric α_1 GlyR (18). PTX must interact with the fully-liganded open state since the channel mean open time was decreased when PTX concentration was increased (figure 5) giving an estimated association rate constant for PTX of 11.6 $\mu M^{-1}s^{-1}$ (figure 5D). PTX had no effect when applied immediately before glycine, which indicates that PTX cannot directly bind to the unliganded receptor, but when PTX was applied during the deactivation phase of glycine-elicited current, the activation phase of the current was lengthened even when glycine was applied 60 s after PTX washout (figure 8C). This could be explained by a trapping mechanism when glycine dissociates before PTX (14). This was simulated by adding a glycine-unbound state (A_3+PC) linked to the sequential glycine-bound closed states (A_2+APC, A+A_2PC and A_3PC) to which PTX remains bound (figures 9B and C). Adding these bound states also accounted for the acceleration of the relaxation of GlyR evoked by PTX, as previously proposed for PTX-evoked $GABA_C$ receptor inhibition (17). To be consistent with the GlyR model describing GlyR kinetics in the absence of PTX, each glycine-bound state associated with PTX (A_2+APC , A+A_2PC , A_3PC) must be linked to a desensitization state (figures 9B, C and D).

In the PTX block models we envisioned, PTX binds within the vestibule of the channel, which shortens channel opening (A_3O to A_3PB see figure 9B). It is then trapped at its binding site when the channel goes back to its closed-state conformation (A_3PB to A_3PC; figure 9B). In these models glycine can unbind while PTX remains trapped.

Two PTX block model subtypes were tested. In model 1(figure 9B), the only way for PTX to bind and unbind is from the open state. The second type of model (model 2 and model 3; figures 9C and D) supposes that the PTX binding site is not fully masked when the channel is in its bound closed conformation. This is also the case for $GABA_C$ receptors (17). In model 2, one step was incorporated between the fully-glycine-liganded closed states (A_3C) and the corresponding glycine-liganded closed states plus PTX (A_3PC). Accordingly, this model contains one cyclic scheme (figure 9C). This model supposes that PTX can escape from its binding site only when GlyR is fully liganded. In model 3, PTX is trapped when the receptor goes back to its unbound closed state. In this model, three steps were incorporated between the glycine-liganded closed states (A_2+ AC, A+A_2C, A_3C) and the corresponding glycine-liganded closed states plus PTX (A_2+ APC, A+A_2PC, A_3PC). Accordingly, this model contains three cyclic schemes (figure 9D). This model is somewhat similar to the kinetic model proposed for $GABA_C$ receptors (17).

To compare the different models accounting for PTX inhibition, we fitted experimental traces obtained by long application of 0.3 mM or 30 mM glycine in the presence of 1, 3 and 10 μM PTX (n = 12 patches). All rate constants estimated with the control model for GlyR were set as fixed parameters. For simplicity, the glycine association rate constant (kon) linking the different glycine-bound states plus PTX (A_2+ APC, A+A_2PC, A_3PC), the desensitization rate constants and the corresponding recovery rate constants linking the liganded closed states plus PTX and the desensitization states (A_2+ APD, A+A_2PD, A_3PD) were also set as fixed variables. All other parameters were set as free variables. We imposed constraints depending on the model tested. Model 1 had no constraint but model 2 and model 3 must have constrained reactions depending on the reaction cycles to satisfy the principle of microscopic reversibility (34). In model 3, the on reactions and the off reactions linking the liganded closed states with and without PTX were set as equivalent (A_2+AC to A_2+APC; A+A_2C to A+A_2PC and A_3C to A_3PC, respectively). Such a simplification postulating that PTX affinity is similar for the three bound closed states of the

receptor was also proposed for $GABA_C$ receptors (17). It is however important to note that when these reactions were set as independent the fit of the experimental traces was not improved and the rate constants for these steps diverged considerably.

As shown in figure 10A, model 1 failed to describe the experimental data (k_{onp} = 7.28 ± 1.73 μM^{-1} s^{-1}, k_{offp} = 72.78 ± 27.9 s^{-1}, a = 2.597 × 10^9 ± 1.753 × 10^8 s^{-1} and b = 2.597 × 10^{11} ± 9.556 × 10^9 s^{-1}). It always predicted a prominent peak current at the onset of the glycine-evoked current, before PTX inhibition can stabilize. This can be overcome by increasing the dissociation rate constant for PTX at a value close to the opening rate constant of the channel (33). But in this case the model predicts a large rebound current even when the association rate constant for PTX was set to maintain a good prediction of PTX IC_{50} value. This was not observed experimentally.

Model 2 (figure 9 C) provided a better prediction of our experimental results. This model gave × 5 ± 0.8 times significant lower SSEs value than model 1 (ANOVA, $P < 0.01$). Incorporating steps for PTX binding to the other liganded bound states (model 3; figure 9D) did not significantly improve the fit when compared to model 2 (ANOVA, $P > 0.1$), suggesting that although such transitions could exist, they were not necessary to describe our experimental data. The optimal averaged rate constant values obtained for models 2 and 3 are listed in Table 1. As shown in table 1, fits of experimental data with model 2 and model 3 gave very similar values for PTX association and dissociation rate constants. In model 2 and model 3, the affinity of PTX for the channel open state (model 2: koff1p/Kon1p = 9.6 μM; model 3: koff1p/Kon1p = 10.7 μM) was found to be lower than that for the bound closed state (model 2: koff2p/Kon2p = 1.6 μM; model 3: koff2p/Kon2p = 1.2 μM). When we attempted to set the affinity of PTX for the channel open state equal to that for the liganded closed states, the SSEs of the fit was 3.1 ± 0.7 times significantly higher (ANOVA, $P < 0.01$), suggesting that the rate constant values for these PTX binding steps are unlikely to be equivalent. A similar conclusion was reported for PTX inhibition of $GABA_C$ receptors (17). Because channel gating must involve large conformational changes, it is reasonable to suppose that the access of PTX to its binding site will be different when the receptor is in a bound closed conformation and in a bound open conformation (17).

Figure 10 shows examples of fits of experimental traces using model 2 (thick dark lines) to responses evoked by the co-application of 30 mM glycine and 10 μM PTX (figure 10A) or 0.3 mM glycine and 1, 3, and 10 μM PTX (figure 10B). The model predicts a stable current amplitude in the presence of 30 mM glycine and 10 μM PTX and a small rebound current at the end of the co-application of PTX and glycine occurring for PTX concentration ≥ 3 μM (figures 10 A and B). The model also predicts an increase in PTX IC_{50} when glycine concentration is increased (figure 10 C). Parameters listed in table 1 predict a PTX IC_{50} of 3.4 μM and of 9.3 μM in the presence of 0.3 mM glycine and 30 mM glycine, respectively. This is in good agreement with our experimental data (2.7 μM and 6.4 μM, respectively; figure 1B). When the rate constant for PTX association from the open state was set as a free parameter, it was close to 5 $\mu M^{-1}s^{-1}$ (Table 1), which is in reasonably good agreement with our experimental measurements (11.5 μM^{-1} s^{-1}). This model also predicts the acceleration of the relaxation phase of the glycine-evoked current observed in the continuous presence of PTX (figure 10 D), the lengthening of the rise time of the 30 mM glycine-evoked current (figure 10 F) during continuous application of PTX and the lack of PTX effect on the rise time of currents evoked by 0.3 mM glycine (figure 10 E). It also predicts the lengthening of the rise time of the glycine-evoked current when PTX was applied during the deactivation phase of the preceding response (figure 10 G). Overall, these data indicate that model 2 characterized by the presence of two PTX binding steps, one from the fully-liganded closed state and one from the open state, is the minimal stochastic scheme that best predicts PTX inhibitory effects on homomeric α_2 GlyRs.

Discussion

In the present study, we demonstrated several unexpected new features for PTX inhibition of wild-type homomeric α_2 GlyR recorded on outside-out patches. As previously observed, PTX had both competitive and non-competitive inhibitory effects on homomeric GlyRs. This complex inhibitory mechanism can be predicted by a simple kinetic model in which glycine can dissociate while PTX remains bound. PTX cannot bind to the GlyR unliganded-closed conformation but our results also suggest that PTX is likely to be trapped while glycine dissociates from the wild-type homomeric α_2 GlyR.

A minimal kinetic model for PTX block

Although kinetic schemes have been proposed to describe the mechanism of PTX inhibition of $GABA_A$ and $GABA_C$ receptors (17, 35), this has not been the case for homomeric GlyRs. The model (model 2, figure 9C) we proposed to describe PTX-evoked GlyR inhibition predicts our experimental data and gives a good prediction of both competitive and noncompetitive mechanisms previously described for homomeric α_1 GlyRs (18). This model is, however, not identical to that recently proposed for PTX inhibition of $GABA_C$ receptors (17). In the $GABA_C$ model there is no intermediate step between the PTX-bound open channel state and the PTX-bound fully-liganded closed state, which results in a reaction cycle with three steps only (17). Such a reaction cycle also

supposes that PTX binding to the open conformation and the receptor conformational change leading to channel closure occur simultaneously. Although a reaction cycle with three steps is computationally valid, it is not physically plausible at least for PTX inhibition of homomeric α_2 GlyR, if one assumes that PTX must bind first before being trapped when the channel closes. This implies a reaction cycle with four steps as shown in figure 9. Accordingly, the receptor first undergoes a conformational change to a new stable state when it is fully liganded (channel opens), PTX binds to the open conformation and then the channel closes. The cycle is terminated when PTX dissociates directly from the fully-liganded closed conformation. However, it should be noted that the estimated off-rate and on-rate constants of the change in the GlyR channel conformation after PTX binding are very fast ($>10^8$ s^{-1}), which could indicate that the two steps (PTX binding and channel closure) collapse. If so, PTX binding might specifically evoke a fast change in GlyR conformation leading to channel closure. This is consistent with what is known about the mechanisms proposed for PTX inhibition of homomeric GlyR. It is now well established that agonist binding causes conformational changes in the extracellular ligand-binding domain which are transmitted to the channel gate via conformational changes in the M2-M3 loop of the GlyR α subunit (4). PTX binding was recently proposed to alter GlyR M2-M3 conformational changes in a way that cannot be achieved by glycine (14). Unlike what has been postulated for the mechanism of PTX inhibition of $GABA_C$ (17), it was not necessary to assume that glycine affinity changes (glycine kon or koff) in the presence of PTX to fit our experimental data. This is consistent with previously published data showing that PTX did not change glycine binding to homomeric GlyRs (18).

Models 1, 2 and 3 predict the previously described "competitive" and "noncompetitive" mechanisms of PTX action on homomeric GlyRs (18), as also described for $GABA_C$ receptors (17). The rebound current after termination of PTX and glycine co-application we observed and the PTX concentration-dependent decrease in the GlyR mean open time of the GlyR channel are consistent with what is known about open channel blockers (noncompetitive mechanism). But in all models tested glycine can dissociate from its binding sites while PTX remains bound, as also proposed for $GABA_C$ receptors (17). This mechanism accounts for the apparent competitive PTX inhibition described for both GlyRs (18) and $GABA_C$ receptors (17). This is not surprising because the recovery from PTX block depends on the PTX dissociation rate constant and on the different glycine-binding steps in the presence of PTX. Accordingly, an increase in glycine concentration will increase the glycine association rate between the glycine-bound closed states plus PTX ($A+A_2PC$, A_2+APC and A_3PC; figure 9), which will result in an apparently faster PTX recovery rate. Accordingly, the simple block mechanism of model 1 also predicts a shift to the right of the PTX concentration response curve when glycine concentration is increased. The simulation of PTX inhibition using model 1 predicted PTX IC_{50} values of 3.0 μM and of 11.1 μM in the presence of 0.3 mM and 30 mM glycine, respectively. This is also the case for models 2 and 3.

Location of the PTX binding site: trapped or not trapped.

There is evidence indicating that PTX acts at the highly conserved M2 domain since several M2 residues have been identified that, when mutated, impair PTX sensitivity (5, 6, 8-13). A series of studies on the $GABA_AR$, $GABA_CR$, GlyR, GluClR and 5-$HT_{3A}R$ established the residues in the cytoplasmic portion of M2 (2' and 6' residues) as crucial determinants of PTX sensitivity (4, 13). Mutations introduced at both the 2' and 6' positions of M2 confer PTX resistance (11). A common feature in all of these studies is that a ring of 6' threonines is invariably required for high PTX sensitivity (6, 8, 11, 14) and it has been suggested that the PTX-binding site probably lies close to 6' pore-lining position of M2 (38). A recent study provided evidence supporting the hypothesis that PTX binds in the pore of the channel (14). PTX is converted into a use-dependent blocker of this GlyR subtype by mutations to R271C and K276C in the M2-M3 loop (14). This was interpreted as a disruption of the M2 structure leading to an even smaller constriction at the pore midpoint allowing PTX to be trapped when the channel closes (14). Our results also support the hypothesis that PTX can bind within the pore of the channel.

Unlike what we observed with the wild-type homomeric α_2 GlyR, there is no evidence that PTX can be trapped in the pore of the wild-type homomeric α_1 GlyR (14). Although GlyR α_1 and α_2 subunits share identical M2-M3 loops and most of the M2 amino acid residue sequence, they differ at the 2' position (39), where glycine is present in the α_1 subunit and alanine in the α_2 subunit. α_1 G254 is an important determinant for PTX sensitivity (11). The 2' residue lies in a narrow part of the pore. Although G254C mutation entirely abolished PTX sensitivity, the α_1 G254A mutation did not impair PTX inhibition, but the Hill coefficient of the PTX concentration-response curve was reduced (11). Moreover, the G254A mutation in the GlyR α_1 subunit dramatically reduces the inhibitory potency of the channel blocker cyanotriphenylborate (40). Homomeric α_1 GlyR and homomeric α_2 GlyR subunits are functionally different. Homomeric α_2 GlyR openings were characterized by a larger single channel conductance (120 pS instead of 80 pS) and a considerably longer mean open time (23), suggesting that the open channel conformation differs between

these two GlyR subtypes. Accordingly, it is tempting to speculate that the pore of homomeric α_2 GlyR is larger in the open state than that of homomeric α_1 GlyR. If so, PTX could go deeper within the pore, which will allow PTX to be trapped when the channel closes.

How many binding sites for PTX?

An unexpected result obtained by fitting our experimental data with kinetic models is that although PTX can be trapped within the channel, it can dissociate from the ligand-bound closed state(s) of the receptors. There is evidence for both $GABA_A$ and $GABA_C$ receptors that PTX binds preferentially to the agonist-bound conformation of the receptor and stabilizes the channel in the closed states (16, 17). Modeling PTX binding to ligand-bound closed states and a ligand-bound open state was necessary to provide a reasonable fit of our experimental data. Model 1 failed to predict the time-course of the glycine-evoked response in the presence of PTX (see figure 10A). Our experimental data also provided direct evidence that PTX cannot directly bind to the unliganded closed conformation, indicating that PTX binds preferentially to the agonist-bound conformation of homomeric α_2 GlyRs.

Models 2 and 3 fitted our experimental data equally well. Moreover, the estimated association and dissociation rate constants for PTX were similar in the two models. Accordingly, it is statistically reasonable to choose the simplest model describing the PTX inhibitory effects. Physiologically, we cannot exclude that PTX can bind to all liganded closed states as proposed for $GABA_C$ receptors (17). In any case, both models predict a faster association and dissociation rate constant for PTX for the ligand-bound closed state than for the fully-liganded open state. This is in apparent contradiction with the proposed single binding site for PTX on the GlyR (4). Our experiments provide no evidence of the presence of a second PTX binding site of different affinity. Indeed, the PTX concentration-response curve was well fitted by a single isotherm function and the Hill coefficient value is close to one.

The difference in the PTX association and dissociation rate constants between the fully-liganded closed state and the fully-liganded open state could also indicate that the access of PTX to its binding site depends on the GlyR channel conformation. Accordingly, it is possible to suppose that glycine binding evokes a partial GlyR channel conformational change before evoking channel openings (41), leading to partial access of PTX to its binding site. This hypothesis also raises the question of how many bound glycine molecules are necessary to evoke a partial conformational change of the channel. Our kinetic simulations cannot resolve this issue, since models 2 and 3 equally predict PTX block mechanisms.

In conclusion, the crucial insight of this study is that PTX acts as a simple channel blocker that can be trapped within the pore of the channel when glycine dissociates from its binding sites. This mechanism accounts for both the previously described competitive and noncompetitive mechanisms of PTX-evoked GlyR inhibition. It also raises the question of a complex conformational change of the GlyR channel that can unmask the PTX binding site when glycine binds to the receptor.

References

1. Legendre, P. (2001) *Cell. Mol. Life Sci.* **58,** 760-793
2. Grudzinska, J., Schemm, R., Haeger, S., Nicke, A., Schmalzing, G., Betz, H., and Laube, B. (2005) *Neuron* **45,** 727-739
3. Pribilla, I., Takagi, T., Langosch, D., Bormann, J., and Betz, H. (1992) *EMBO J.* **11,** 4305-4311
4. Lynch, J.W. (2004) *Physiol. Rev.* **84,** 1051-1095
5. Ffrench-Constant, R.H., Rocheleau, T.A., Steichen, J.C., and Chalmers, A.E. (1993) *Nature* **363,** 449-451
6. Gurley, D., Amin, J., Ross, P.C., Weiss, D.S., and White, G. (1995) *Receptors Channels* **3,** 13-20
7. Xu, M., Covey, D.F., and Akabas, M.H. (1995) *Biophys J.* **69,** 1858-1867
8. Zhang, D., Pan, Z.H., Zhang, X., Brideau, A.D., and Lipton, S.A. (1995) *Proc. Natl. Acad. Sci. USA* **92,** 11756-11760
9. Etter, A., Cully, D.F., Liu, K.K., Reiss, B., Vassilatis, D.K., Schaeffer, J.M., and Arena, J.P. (1999) *J. Neurochem.* **72,** 318-326
10. Buhr, A., Wagner, C., Fuchs, K., Sieghart, W., and Sigel, E. (2001) *J. Biol. Chem.* **276,** 7775-7781
11. Shan, Q., Haddrill, J.L., and Lynch, J.W. (2001) *J. Neurochem.* **76,** 1109-1120
12. Dibas, M.I., Gonzales, E.B., Das, P., Bell-Horner, C.L., and Dillon, G.H. (2002) *J. Biol. Chem.* **277,** 9112-9117
13. Das, P., and Dillon, G.H. (2005) *J. Pharmacol. Exp. Ther.* **314,** 320-328
14. Hawthorne, R., and Lynch, J.W. (2005) *J. Biol. Chem.* **280**, 35836-35843.
15. Inoue, M., and Akaike, N. (1988) *Neurosci. Res.* **5,** 380-394
16. Newland, C.F., and Cull-Candy, S.G. (1992) *J. Physiol.* **447,** 191-213
17. Qian, H., Pan, Y., Zhu, Y., and Khalili, P. (2005) *Mol. Pharmacol.* **67,** 470-479
18. Lynch, J.W., Rajendra, S., Barry, P.H., and Schofield, P.R. (1995) *J. Biol. Chem.* **270,** 13799-13806
19. Legendre, P. (1997) *J. Neurophysiol.* **77,** 2400-2415
20. Yoon, K.W., Wotring, V.E., and Fuse, T. (1998) *Neuroscience* **87,** 807-815
21. Kuhse, J., Kuryatov, A., Maulet, Y., Malosio, M.L., Schmieden, V., and Betz, H. (1991) *FEBS Lett.* **283,** 73-77
22. Triller, A., Seitanidou, T., Franksson, O., and Korn, H. (1990) *New Biol.* **2,** 637-641
23. Mangin, J.M., Baloul, M., Prado De Carvalho, L., Rogister, B., Rigo, J.M., and Legendre, P. (2003) *J. Physiol.* **553,** 369-386
24. Flint, A.C., Liu, X., and Kriegstein, A.R. (1998) *Neuron* **20,** 43-53
25. Mangin, J.M., Nguyen, L., Gougnard, C., Hans, G., Rogister, B., Belachew, S., Moonen, G., Legendre, P. and Rigo, J.M. (2005) *Mol. Pharmacol.* **67,** 1783-1796
26. Hamill, O.P., Marty, A., Neher, E., Sakmann, B., and Sigworth, F.J. (1981) *Pflugers Arch.* **391,** 85-100
27. Franke, C., Hatt, H., and Dudel, J. (1987) *Neurosci. Lett.* **77,** 199-204
28. Legendre, P. (1998) *J. Neurosci.* **18,** 2856-2870
29. Clements, J.D., and Westbrook, G.L. (1991) *Neuron* **7,** 605-613
30. Aldrich, R.W., Corey, D.P., and Stevens, C.F. (1983) *Nature* **306,** 436-441
31. Sigworth, F.J., and Sine, S.M. (1987) *Biophys J.* **52,** 1047-1054
32. Maconochie, D.J., and Steinbach, J.H. (1995) *J. Gen. Physiol.* **106,** 113-147
33. Legendre, P., Ali, D.W., and Drapeau, P. (2000) *J. Neurosci.* **20,** 140-148
34. Colquhoun, D., and Hawkes, A.G. (1995) *Single-channel recording,* 2nd Ed., Sakmann, B., and Neher, E. eds, 397-479, Plenum press, NY
35. Adelsberger, H., Brunswieck, S., and Dudel, J. (1998) *Eur. J. Neurosci.* **10,** 179-187
36. Burzomato, V., Beato, M., Groot-Kormelink, P.J., Colquhoun, D., and Sivilotti, L.G. (2004) *J. Neurosci.* **24,** 10924-10940
37. Gentet, L.J., and Clements, J.D. (2002) *J Physiol* **544,** 97-106
38. Zhorov, B.S., and Bregestovski, P.D. (2000) *Biophys J.* **78,** 1786-1803
39. Harvey, R.J., Schmieden, V., Von Holst, A., Laube, B., Rohrer, H., and Betz, H. (2000) *Eur. J. Neurosci.* **12,** 994-1001
40. Rundstrom, N., Schmieden, V., Betz, H., Bormann, J., and Langosch, D. (1994) *Proc. Natl. Acad. Sci. USA* **91,** 8950-8954
41. Colquhoun, D., and Sivilotti, L.G. (2004) *Trends Neurosci.* **27,** 337-344

Footnotes

This work was supported by INSERM, CNRS, NRJ funding, Association Française contre les Myopathies (AFM) and INSERM - CFB agreement (P. Legendre and J.M. Rigo). Dian-Shi Wang is supported by the Human Frontier Science Program Short-Term Fellowship and International Brain Research Organization Research Fellowship. We thank Drs. Richard Miles, John D. Clements, Hervé Le Corronc and Emilie Muller for helpful discussions and technical assistance.

The abbreviations used are: ANOVA, analysis of variance; CHO, Chinese hamster ovary; DMSO, dimethyl sulfoxide; FL, first latency; $GABA_AR$, γ-aminobutyric acid type A receptor; $GABA_CR$, γ-aminobutyric acid type C receptor; GluClR, glutamate receptor chloride channel; GlyR, glycine receptor; *I-V*, curren-voltage; PTX, picrotoxin; V_H, holding potential; *V*r, reversal potential; τ_{decay}, deactivation time constant; τ_{fast}, fast rising time constant; τ_{slow}, slow rising time constant.

Table 1. Kinetic parameters for PTX inhibition derived from models 2 and 3 fitting (mean ± SE, *n* = 12).

	MODEL 2	MODEL 3
k_{on}	0.77 ± 0.04 μM^{-1} s^{-1}	0.77 ± 0.04 μM^{-1} s^{-1}
k_{off1}	1657.9 ± 404.5 s^{-1}	1657.9 ± 404.5 s^{-1}
k_{off2}	76.6 ± 47.4 s^{-1}	76.6 ± 47.4 s^{-1}
k_{off3}	2853.6 ± 263.7 s^{-1}	2853.6 ± 263.7 s^{-1}
d1	1579.8 ± 683.2 s^{-1}	1579.8 ± 683.2 s^{-1}
d2	711.3 ± 309.3 s^{-1}	711.3 ± 309.3 s^{-1}
d3	11.75 ± 2.3 s^{-1}	11.75 ± 2.3 s^{-1}
r1	94.5 ± 44.9 s^{-1}	94.5 ± 44.9 s^{-1}
r2	461 ± 123.8 s^{-1}	461 ± 123.8 s^{-1}
r3	0.1 ± 0.02 s^{-1}	0.1 ± 0.02 s^{-1}
α	21.8 ± 1.3 s^{-1}	21.8 ± 1.3 s^{-1}
β	4875 ± 89.7 s^{-1}	4875 ± 89.7 s^{-1}
k_{on1p}	4.9 ± 0.9 μM^{-1} s^{-1}	5.4 ± 0.9 μM^{-1} s^{-1}
k_{off1p}	46.9 ± 11.9 s^{-1}	57.8 ± 10.3 s^{-1}
k_{on2p}	483.5 ± 121.4 μM^{-1} s^{-1}	278 ± 69.4 μM^{-1} s^{-1}
k_{off2p}	749.8 ± 198.3 s^{-1}	327.9 ± 83.6 s^{-1}
a	$3.069 \times 10^{8} \pm 2.741 \times 10^{8}$ s^{-1}	$2.009 \times 10^{8} \pm 8.186 \times 10^{7}$ s^{-1}
b	$7.423 \times 10^{9} \pm 5.029 \times 10^{8}$ s^{-1}	$3.363 \times 10^{9} \pm 1.572 \times 10^{9}$ s^{-1}

Figure legends

Figure 1. Concentration-dependent inhibition of α_2 homomeric GlyR by PTX.
A) Outside-out patch clamp recordings showing inhibition of 300 μM and 30 mM glycine-activated currents evoked by the indicated concentrations of co-application of PTX in CHO cells transfected with the α_2 GlyR subunit. Each trace represents the average of 15-30 responses. Note that when the PTX concentration was > 1 μM the small transient rebound current was always induced during the withdrawal of the two drugs. The left and right traces were obtained from two different patches. The thick line represents the application of drugs. B) PTX inhibition curves for 300 μM (●) and 30 mM (○) glycine-evoked responses. Currents were normalized to the responses in the absence of PTX. Each point is the average of values from 5-12 cells. In most instances multiple concentrations (three) of PTX were applied to the same cell. Data were fitted with the Hill equation (see Materials and Methods) giving an IC_{50} of 2.7 ± 0.2 μM and a Hill coefficient of 0.8 ± 0.04 for 300 μM glycine, and an IC_{50} of 6.4 ± 0.6 μM and a Hill coefficient of 0.8 ± 0.05 for 30 mM glycine.

Figure 2. Voltage-independent inhibition of glycine response by PTX.
A) Responses to 300 μM glycine (Control) and to co-application of 300 μM glycine and 10 μM PTX (glycine + 10 μM PTX) at V_H of + 50 and - 50 mV. Note that the rebound currents at both + 50 and - 50 mV are similar. Each trace represents the average of 10-12 trials. The thick line represents the application of 300 μM glycine. B) The current-voltage relationships of glycine responses induced by 300 μM glycine in the absence (●) and presence (■) of simultaneous application of 10 μM PTX. Note that the inhibitory effect of PTX is similar at all V_H values. The reversal potentials of glycine-activated currents are 2.9 mV for glycine and 4.2 mV for glycine + PTX. Currents were normalized to the response induced by 300 μM glycine alone at a V_H of - 50 mV (*). Each point is the mean of values from 5-10 cells. C) Plot of the percentage of block by co-application of 300 μM glycine and 10 μM PTX as a function of the holding potentials. Data were averaged from 5-10 cells and fitted by linear regression.

Figure 3. Acceleration of decay phase of glycine-activated current by the continuous presence of PTX.
A1) Current traces activated by 300 μM glycine (control), by co-application of 300 μM glycine and 10 μM PTX (+ 10 μM PTX), and by 300 μM glycine in the continuous presence of 10 μM PTX (+ continuous PTX) when PTX was maintained before, during and after glycine application. Each trace represents the average of 12-15 responses. Note that the glycine-elicited currents in the control condition and with co-application of PTX returned slowly to the baseline after termination of glycine application, whereas the continuous presence of PTX eliminated the rebound current and significantly accelerated the decay phase. The thick line represents the application of 300 μM glycine. A2) Normalized decay phase of glycine responses replotted on an expanded time scale to illustrate better the acceleration of the deactivation time-course by continuous 10 μM PTX. The decay phase was best fitted with a single exponential function giving a decay time constant of 114 ms for control response, 116 ms for co-application of glycine and PTX, and 27 ms for continuous presence of PTX. Similar results were obtained from another 12 cells. B1) Normalized responses evoked by short pulses (1 ms) of 30 mM glycine in the absence and presence of various concentrations of continuous PTX (shown beside each trace in μM). Note that the deactivation time constants decreased in a concentration-dependent manner. Each trace represents the average of 15-30 responses. B2) Summary results for the deactivation time constants obtained from four different concentrations of PTX. ANOVA analysis indicated significant statistical differences (P < 0.01) among data groups. A and B were obtained from different patches.

Figure 4. Decrease in mean open time in the continuous presence of PTX
A-B) Representative, non-consecutive, single-channel openings of a single α_2 homomeric GlyR evoked by repetitive short pulses (1 ms) of 30 mM glycine in the absence (A) and presence (B) of continuous 10 μM PTX on the same patch (cut-off filter frequency, 2 kHz). The thick line represents the application of 10 μM PTX. Ensemble-averaged currents (lower traces; n = 116 for 30 mM glycine, n = 202 for + 10 μM PTX) obtained from 7-9 different experiments were best fitted with a single exponential function (smooth lines). Decay time constants are indicated for both 30 mM glycine and + 10 μM PTX. C-D) Open time duration histograms obtained in the control (30 mM glycine; C) and in the continuous presence of 10 μM PTX (D) are shown as a function of log intervals with the ordinate on a square root scale. Histograms were better fitted with 1 exponential curve. Mean open time was decreased from 48.4 ms in the control condition to 6.1 ms in the continuous presence of PTX. E-F) Closed time histograms in the control (30 mM glycine; E) and in the continuous presence of 10 μM PTX (F) were obtained. Histograms are shown as a function of log intervals, with the ordinate on a square root scale. The distributions were fitted with 1 and 2 exponential curves for the control

and in the continuous presence of PTX, respectively. Note that τ_{c1} = 0.23 ms is very similar to the closed time constant τ_c = 0.27 ms in the control conditions, whereas τ_{c2} = 5.76 ms is apparent in the continuous presence of PTX.

Figure 5. PTX decreased the mean open time of GlyR in a concentration-dependent manner.
A-C) Open time duration histograms obtained in the control (30 mM glycine; A) and in the continuous presence of 3 μM PTX (B), 10 μM PTX (C) are shown as a function of log intervals with the ordinate on a square root scale. Histograms were better fitted with 1 exponential curve. Note that mean open time was decreased by PTX in a concentration-dependent manner. D) The reciprocals of the mean open times were plotted as a function of the PTX concentration, and the binding (k_{on}) and closing (β) rate constants were calculated from the relationship $1/\tau_b = [PTX]k_{on} + \beta$, where τ_b is the mean open time and [PTX] is the PTX concentration. The linear fit to the data gave k_{on} value of 11.6 $\mu M^{-1}s^{-1}$ and β value of 27.9 s^{-1}. Mean open times were obtained by pooling single-channel currents (22-66 trials) in 1-3 different experiments for each concentration of PTX.

Figure 6. Slower onset of macroscopic currents activated by saturating concentration of glycine in the continuous presence of PTX.
A) Averaged traces of currents (n = 10-25) obtained from the same patch showing the activation phase of the responses evoked by 300 μM glycine, co-application of 300 μM glycine and 10 μM PTX (+10 μM PTX), and by glycine in the continuous presence of 10 μM PTX (+ continuous PTX). B) Summary of data (n = 12-14) obtained from the experiments shown in A. NS: nonsignificance; * $P < 0.05$. C) Averaged traces of currents (n = 12-15) obtained from the same patch showing the activation phase of the responses activated by saturating concentration of 30 mM glycine, co-application of 30 mM glycine and 10 μM PTX, and by glycine in the continuous presence of 10 μM PTX. Note that the activation phase of the glycine response was slowed down in the continuous presence of PTX. D) Averaged traces of currents (n = 12-25) obtained from the same patch showing the activation phase of the responses evoked by saturating concentration of 30 mM glycine in the absence and presence of continuous 10 μM PTX, and by over-saturating concentration of 100 mM glycine in the absence and presence of continuous 10 μM PTX. Note that increasing glycine concentration to 100 mM does not change the activation time-course of current response activated by 30 mM glycine in the continuous presence of PTX. E-F) Summary of data (n = 8-12) obtained from the experiments shown in C and D (NS: nonsignificance).

Figure 7. Increase in the first latency accounts for the slower onset.
A-B) Representative, non-consecutive, single-channel openings of a single α_2 homomeric GlyR evoked by repetitive 200 ms step applications of 30 mM glycine in the absence (A) and presence (B) of continuous 10 μM PTX on the same patch (cut-off filter frequency, 2 kHz). Ensemble-averaged currents (lower traces; n = 266 for 30 mM glycine, n = 229 for + 10 μM PTX) were best fitted with a bi-exponential function (smooth lines). Fast and slow time constants and their relative areas are indicated for both 30 mM glycine and + 10 μM PTX. C-D) First latency distributions in the absence (C) and presence (D) of continuous application of 10 μM PTX. The first latency distributions were best fitted by the sum of two exponential functions (smooth lines). Fast and slow time constants and their relative weights are indicated for both 30 mM glycine and + 10 μM PTX. Note that the time constants and their relative areas of the first latency distributions are identical to those of the ensemble average currents, indicating that the slower onset of the ensemble average current in the continuous presence of PTX was due to increase in first latency duration.

Figure 8. Channel re-openings were required for recovery from PTX block.
A1) Average of 5 traces of current obtained in response to a 600 ms step application of 10 mM glycine and transiently inhibited by a 300 ms step application of 10 μM PTX with 10 mM glycine. The dashed boxes in A1 indicate parts of the trace enlarged in A2 (left box) and A3 (right box). A2) The onset of the picrotoxin inhibition was well fitted by a mono-exponential curve (gray dashed line) giving a time constant of 12 ms. A3) The recovery from the inhibition by PTX was best fitted by a bi-exponential curve (gray dashed line) giving time constants τ_{fast} = 4 ms (28 %) and τ_{slow} = 37 ms (72 %). B1) Average of 5 traces showing currents evoked by a 300 ms step application of 10 mM glycine following a 300 ms step application of control solution (left black trace) or 10 μM PTX (right gray trace). Dashed boxes in B1 indicate the part of the traces enlarged in B2. B2) The onset of the both responses was best fitted by a bi-exponential function. The fast and slow time constant values and their relative area were respectively indicated in black (control pre-incubation) and in gray (PTX pre-incubation). Note the absence of effect of the PTX pre-incubation. C1) Example of three consecutives responses to 200 ms step application of 10 mM glycine where the first application was directly followed by a 500 ms step application of 10 μM PTX. The delay between each application is indicated between each trace. Note the quickening in the decay of the first glycine response during the PTX application and the slowing down in the onset of the second response. The third response exhibits an onset similar to the first response indicating a complete recovery from

PTX effect. Dashed boxes indicate the part of the two first traces enlarged in C2. C2) The onset of the first and second responses was best fitted by a bi-exponential function. The fast and slow time constant values and their relative area were respectively indicated in black (first application, mean of 5 traces) and gray (second application, mean of 5 traces).

Figure 9. Kinetic schemes used for fitting glycine responses in the absence and presence of PTX.
A indicates agonist, P PTX, C resting states of the receptor, D desensitization state, and O open state. A) This kinetic scheme was used for homomeric α_2 GlyR in control conditions (without PTX). B) In model 1, PTX can bind and unbind from the GlyR open state only. PTX remains bound if continuously applied when glycine dissociates from its binding sites. C) In model 2, PTX can bind and unbind from the fully-glycine-liganded closed state or the open state of GlyR. In this scheme, PTX is trapped when glycine dissociates from the fully-liganded closed state. D) In model 3, PTX can bind and unbind from all glycine-bound states, but PTX is only trapped when the receptor returns to the glycine-unbound closed state.

Figure 10. Prediction of the experimental results by kinetic models.
A) Outside-out currents elicited by glycine (30 mM) in the absence and presence of 10 μM PTX (gray traces) were superimposed to simulated currents using model 1 (gray line) and kinetic model 2 (black) derived traces (V_H = -50 mV). Note that model 1 failed to predict the PTX effect. B) Outside-out currents evoked by co-application of glycine (0.3 mM) and 0, 1, 3 and 10 μM PTX (gray lines) were superimposed to simulated currents using model 2. Model 2 well predicts the concentration-dependent inhibitory effect of PTX and the time-course of glycine-evoked currents in the absence and presence of PTX. C) This model also predicts the shift to the right of the PTX inhibition curve when glycine concentration is increased. The concentration-response curves were obtained from theoretical currents generated using model 2. D) theoretical current obtained with model 2 evoked by 5 ms pulse of 30 mM glycine followed by the application of 0, 1, 3 and 10 μM PTX. Note that this kinetic scheme predicts the PTX-evoked concentration-dependent decrease in the decay phase duration. E) Simulated traces of currents showing the activation phase of the responses evoked by 300 μM glycine, co-application of 300 μM glycine and 10 μM PTX and by glycine in the continuous presence of 10 μM PTX. Note the lack of effect of the continuous application of PTX, when compared to co-application of glycine plus PTX, on the activation phase of simulated glycine-evoked current. F) Simulated traces of currents showing the activation phase of the responses activated by a saturating concentration of 30 mM glycine, co-application of 30 mM glycine and 10 μM PTX, and by glycine in the continuous presence of 10 μM PTX. Model 2 predicts that the activation phase of the glycine response was slowed down in the continuous presence of PTX. G) Simulated traces generated using model 2 showing that this kinetic scheme also predicts that the lengthening of the rise time evoked by PTX can persist up to 60 s after washout of glycine and PTX. For time-course comparisons the control response on the left was superimposed (in gray) on the other simulated glycine-evoked currents.

figure 1

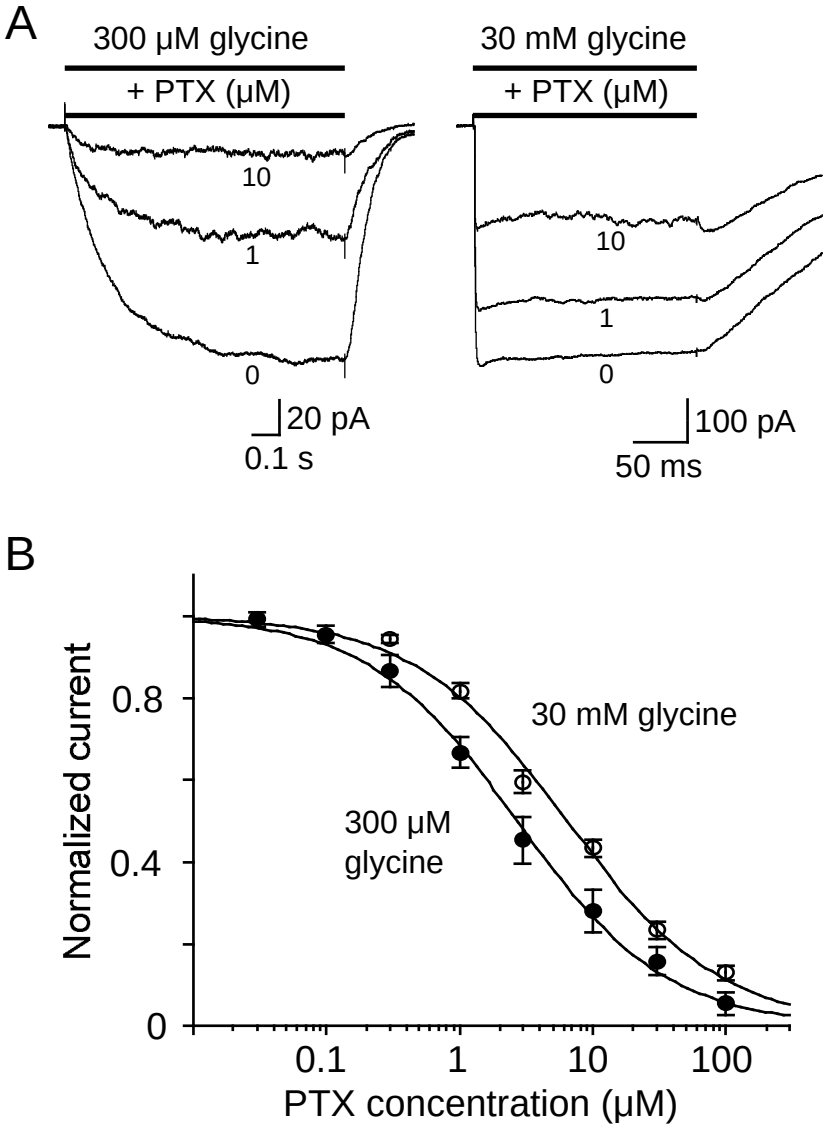
A
300 μM glycine
+ PTX (μM)
10
1
0
20 pA
0.1 s
30 mM glycine
+ PTX (μM)
10
1
0
100 pA
50 ms
B
Normalized current
0.8
0.4
0
0.1
1
10
100
PTX concentration (μM)
30 mM glycine
300 μM
glycine

figure 2

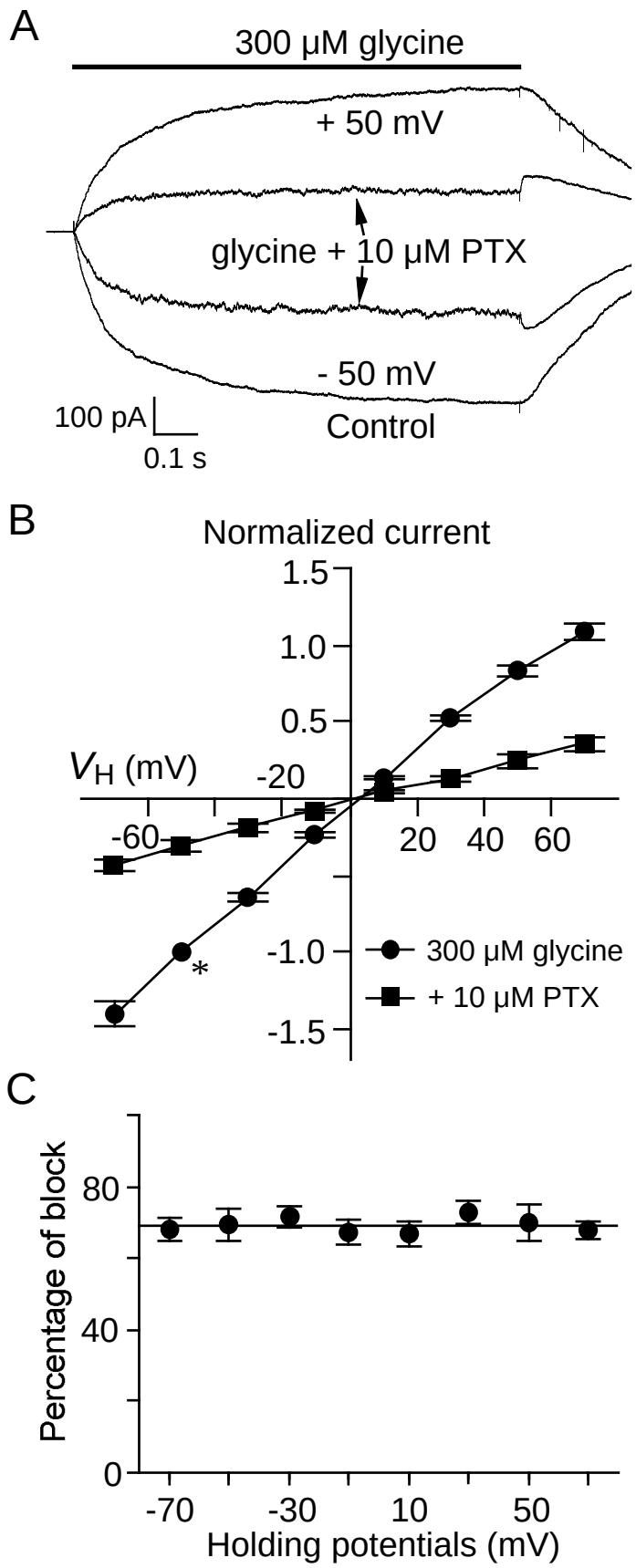
A
300 μM glycine
+ 50 mV
glycine + 10 μM PTX
- 50 mV
100 pA
0.1 s
Control
B
Normalized current
1.5
1.0
0.5
V_H (mV)
-20
-60
20
40
60
-1.0
-1.5
*
300 μM glycine
+ 10 μM PTX
C
Percentage of block
80
40
0
-70
-30
10
50
Holding potentials (mV)

figure 3

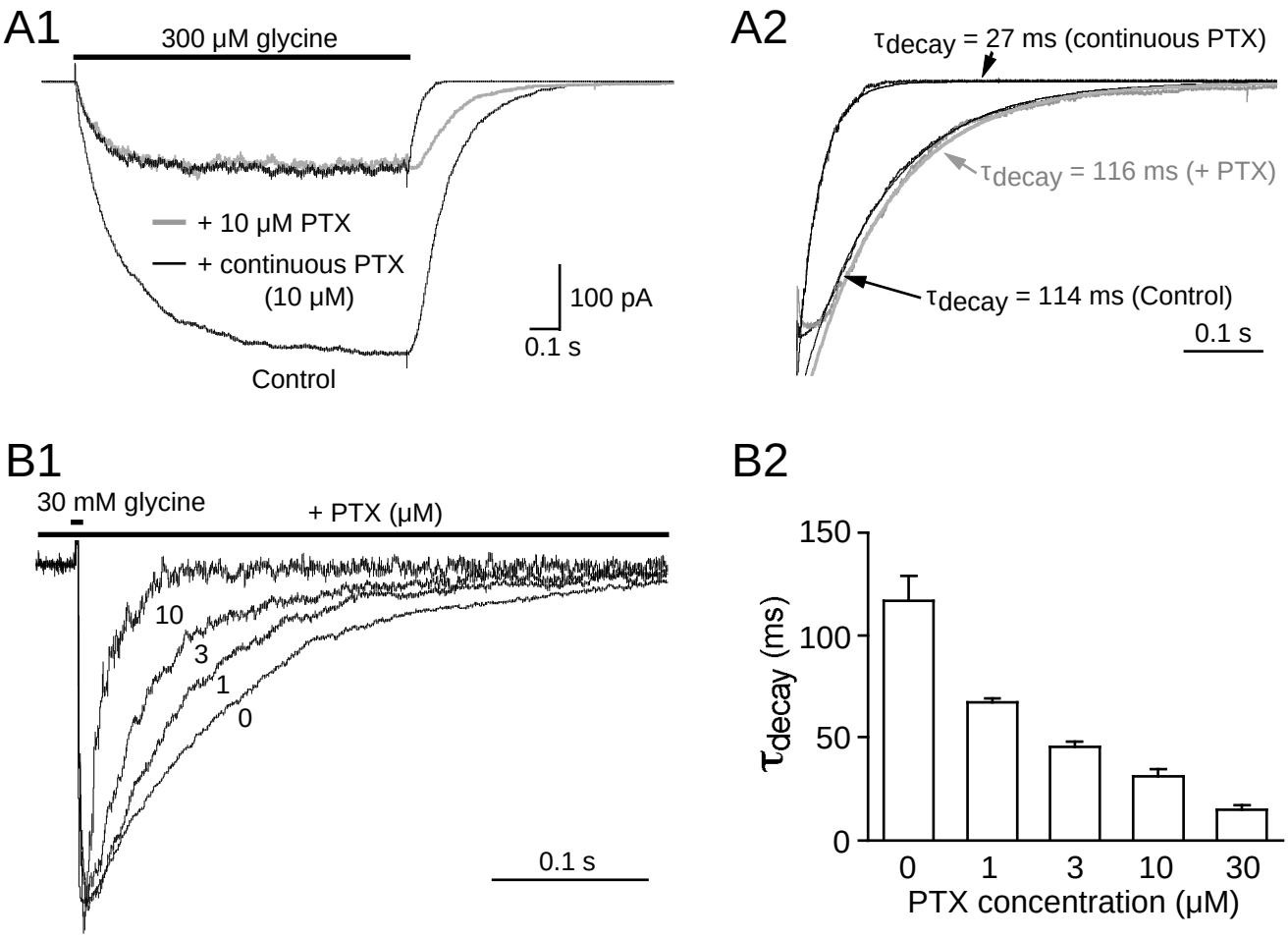
A1
300 μM glycine
+ 10 μM PTX
+ continuous PTX
(10 μM)
100 pA
0.1 s
Control
A2
τdecay = 27 ms (continuous PTX)
τdecay = 116 ms (+ PTX)
τdecay = 114 ms (Control)
0.1 s
B1
30 mM glycine
+ PTX (μM)
10
3
1
0
0.1 s
B2
150
100
50
0
τdecay (ms)
0
1
3
10
30
PTX concentration (μM)

FIGURE 4

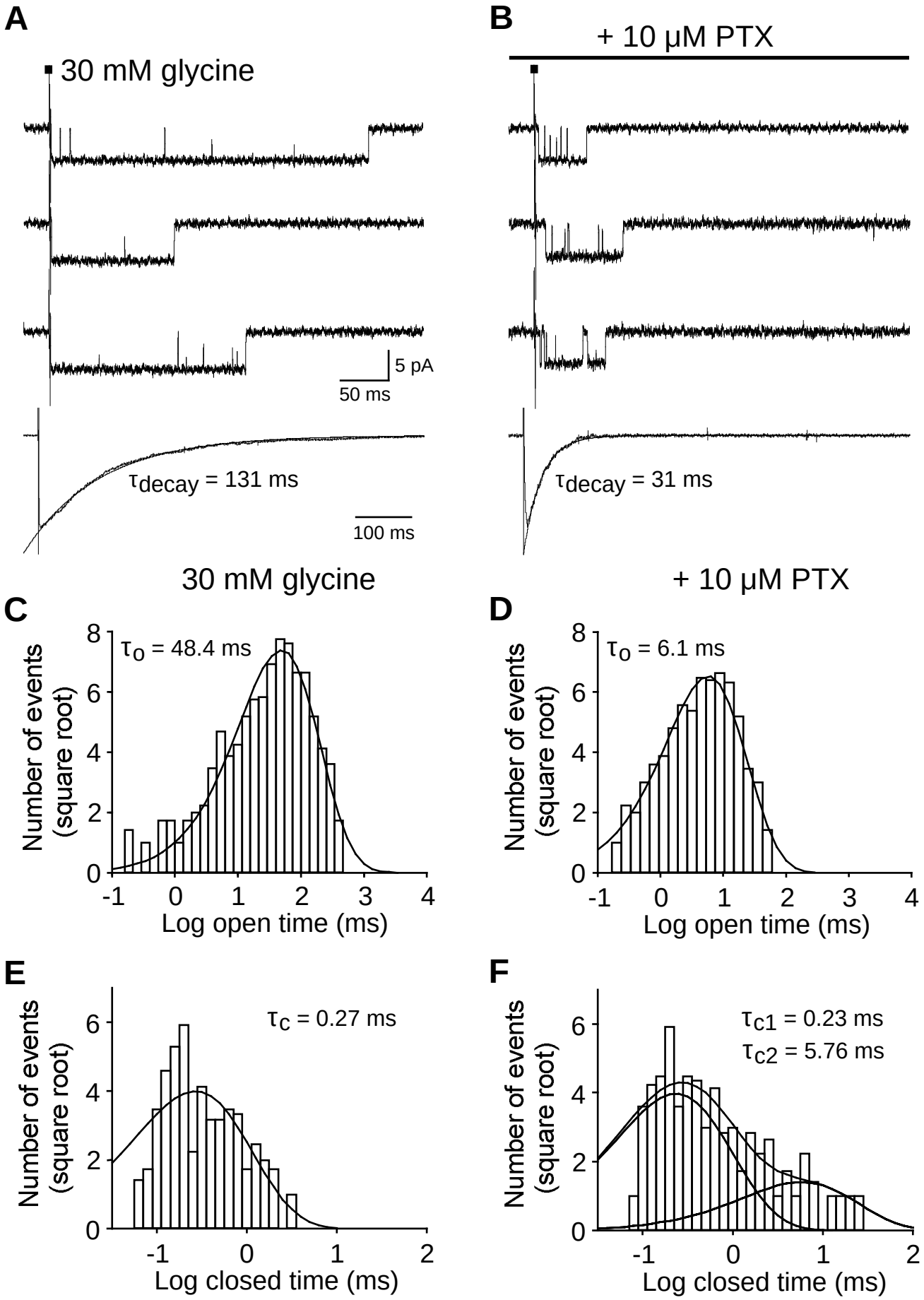
A
30 mM glycine
5 pA
50 ms
τdecay = 131 ms
100 ms
B
+ 10 μM PTX
τdecay = 31 ms
30 mM glycine
+ 10 μM PTX
C
τo = 48.4 ms
Number of events (square root)
Log open time (ms)
D
τo = 6.1 ms
Number of events (square root)
Log open time (ms)
E
τc = 0.27 ms
Number of events (square root)
Log closed time (ms)
F
τc1 = 0.23 ms
τc2 = 5.76 ms
Number of events (square root)
Log closed time (ms)

FIGURE 5

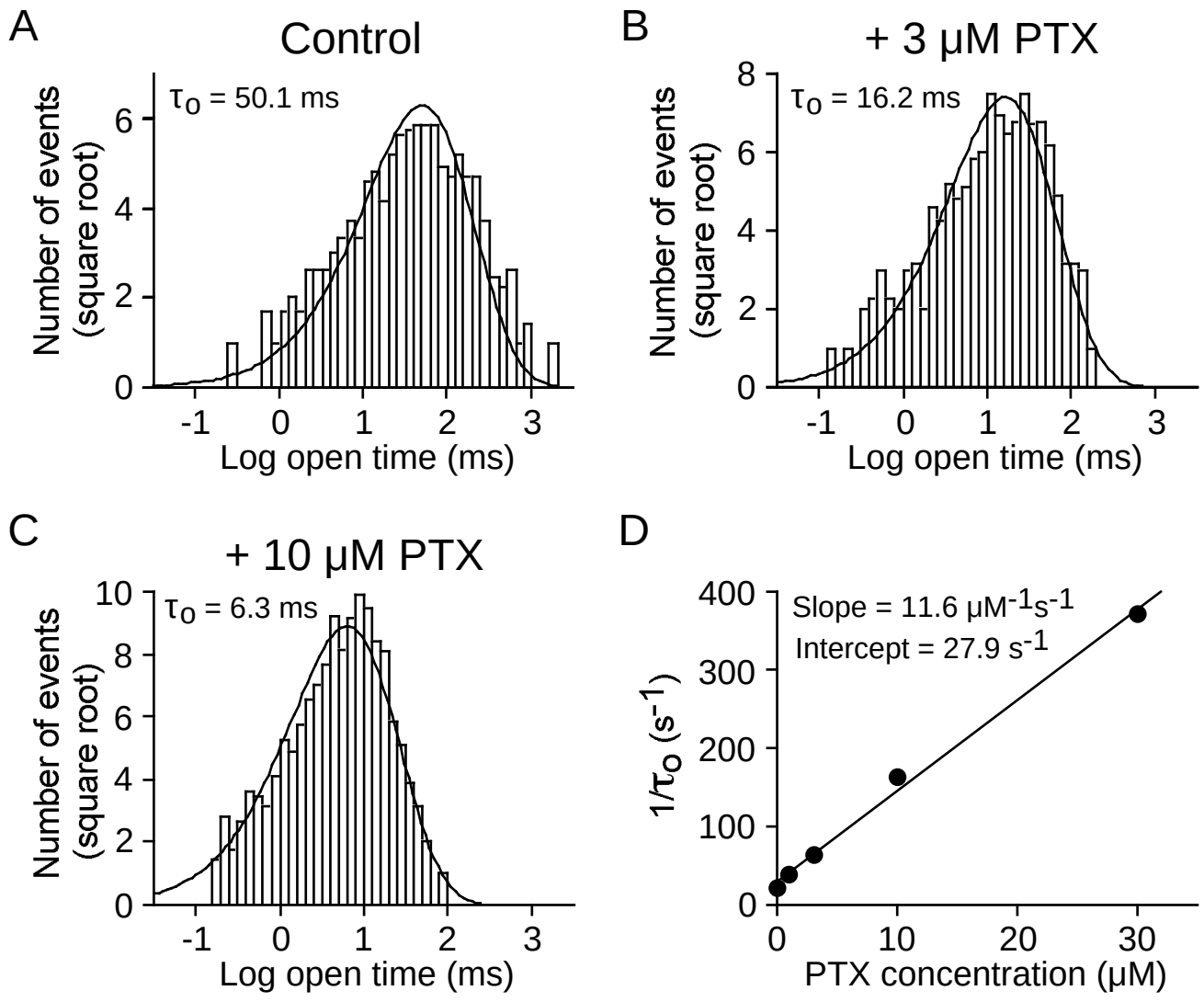
A
Control
τo = 50.1 ms
Number of events (square root)
Log open time (ms)
B
+ 3 μM PTX
τo = 16.2 ms
Number of events (square root)
Log open time (ms)
C
+ 10 μM PTX
τo = 6.3 ms
Number of events (square root)
Log open time (ms)
D
Slope = 11.6 μM-1s-1
Intercept = 27.9 s-1
1/τo (s-1)
PTX concentration (μM)

figure 6

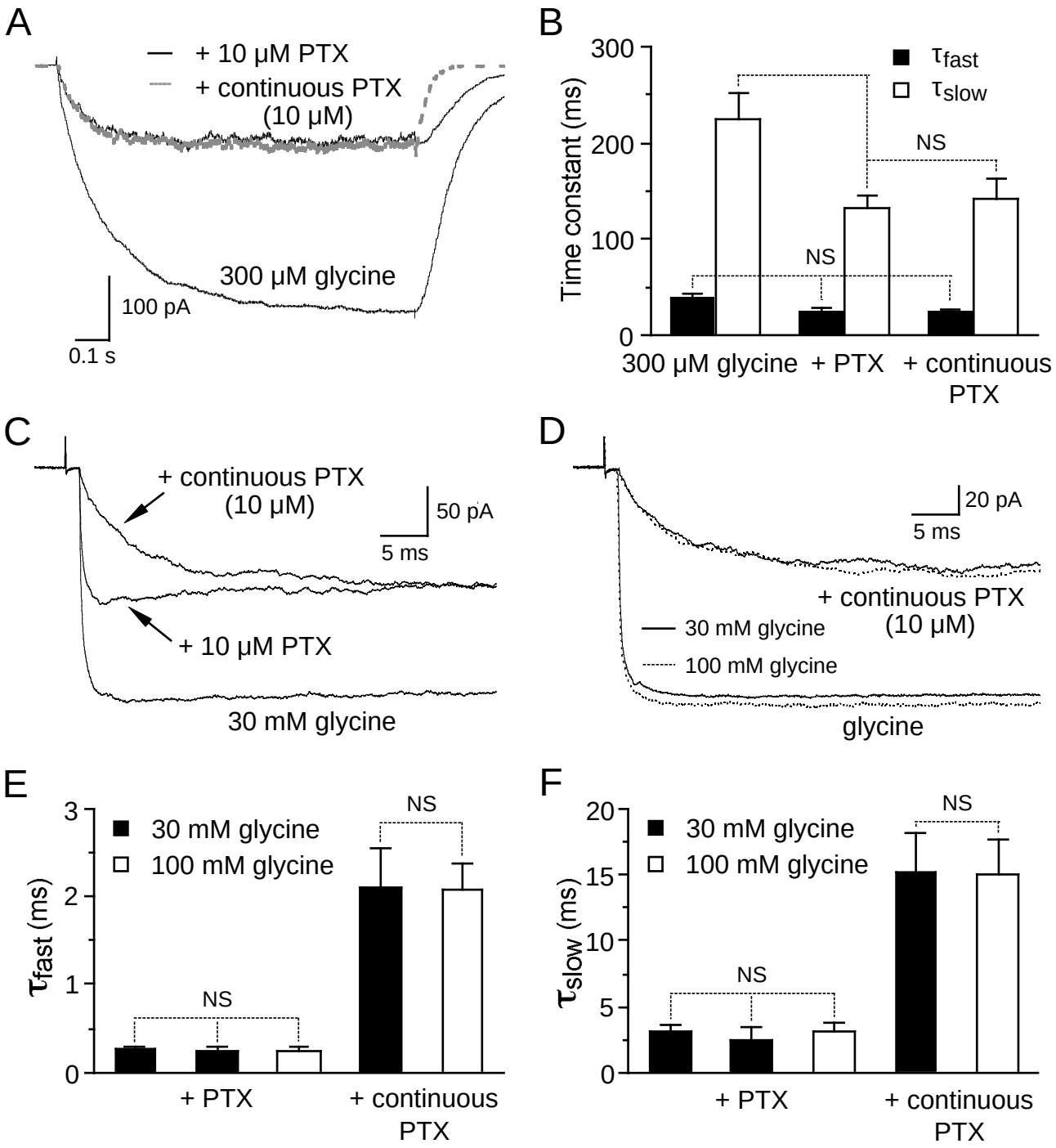
A
+ 10 μM PTX
+ continuous PTX
(10 μM)
300 μM glycine
100 pA
0.1 s
B
Time constant (ms)
300
200
100
0
τfast
τslow
NS
NS
300 μM glycine
+ PTX
+ continuous
PTX
C
+ continuous PTX
(10 μM)
50 pA
5 ms
+ 10 μM PTX
30 mM glycine
D
20 pA
5 ms
+ continuous PTX
(10 μM)
30 mM glycine
100 mM glycine
glycine
E
τfast (ms)
3
2
1
0
30 mM glycine
100 mM glycine
NS
NS
+ PTX
+ continuous
PTX
F
τslow (ms)
20
15
10
5
0
30 mM glycine
100 mM glycine
NS
NS
+ PTX
+ continuous
PTX

figure 7

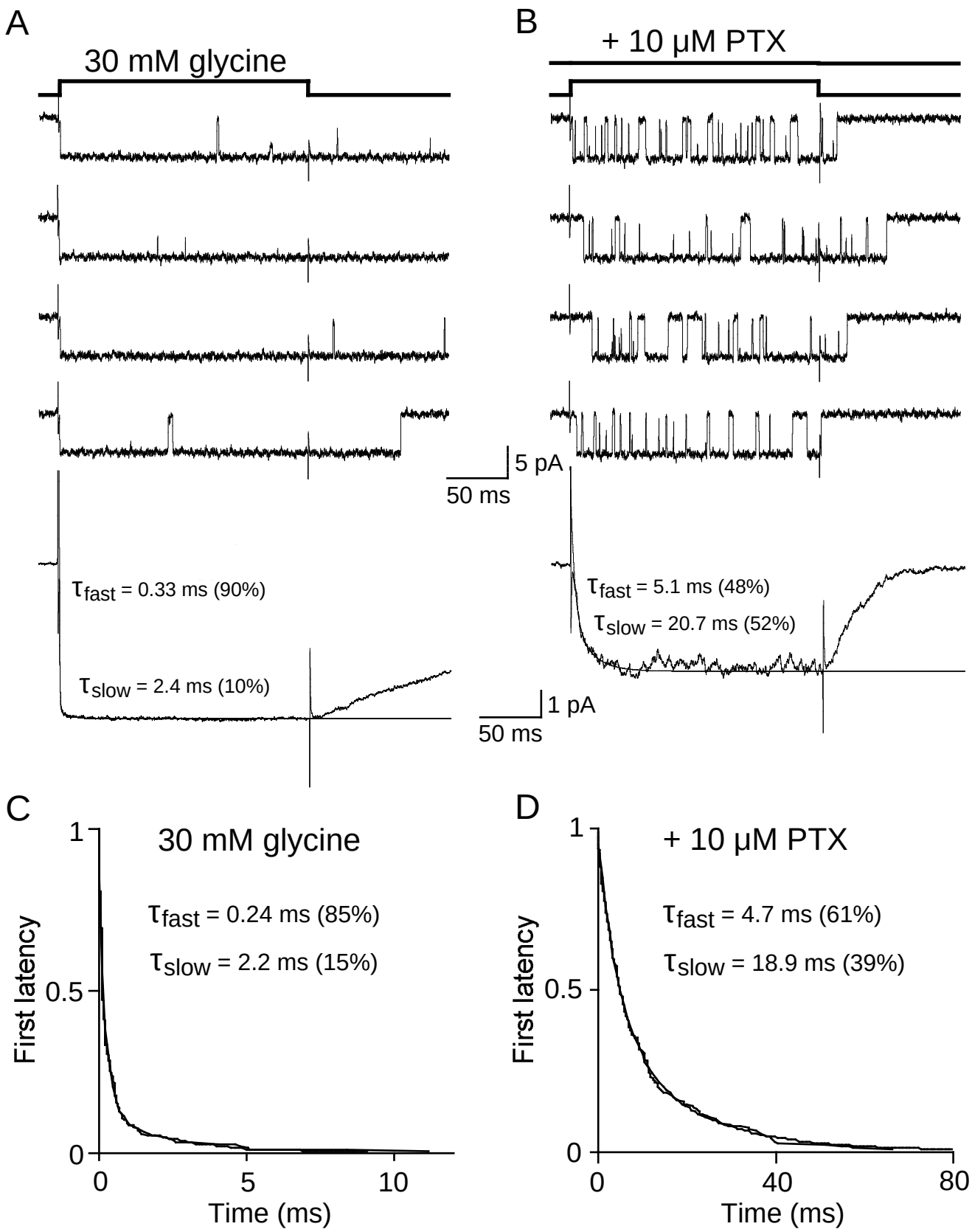
A
30 mM glycine
τfast = 0.33 ms (90%)
τslow = 2.4 ms (10%)
B
+ 10 μM PTX
5 pA
50 ms
τfast = 5.1 ms (48%)
τslow = 20.7 ms (52%)
1 pA
50 ms
C
30 mM glycine
τfast = 0.24 ms (85%)
τslow = 2.2 ms (15%)
First latency
1
0.5
0
0
5
10
Time (ms)
D
+ 10 μM PTX
τfast = 4.7 ms (61%)
τslow = 18.9 ms (39%)
First latency
1
0.5
0
0
40
80
Time (ms)

FIGURE 8

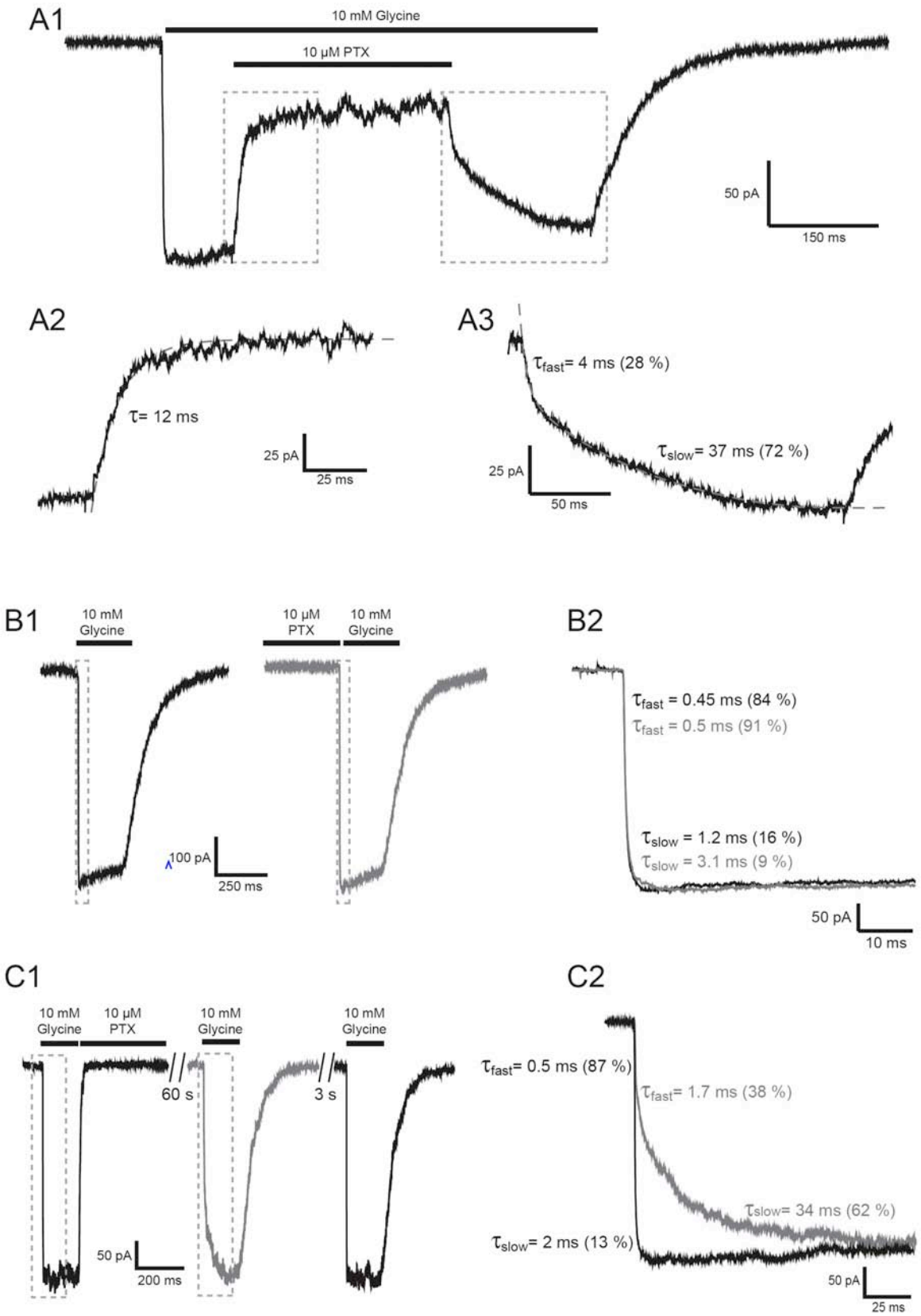
A1
10 mM Glycine
10 µM PTX
50 pA
150 ms
A2
τ= 12 ms
25 pA
25 ms
A3
τfast= 4 ms (28 %)
τslow= 37 ms (72 %)
25 pA
50 ms
B1
10 mM Glycine
10 µM PTX
10 mM Glycine
100 pA
250 ms
B2
τfast = 0.45 ms (84 %)
τfast = 0.5 ms (91 %)
τslow = 1.2 ms (16 %)
τslow = 3.1 ms (9 %)
50 pA
10 ms
C1
10 mM Glycine
10 µM PTX
10 mM Glycine
10 mM Glycine
60 s
3 s
50 pA
200 ms
C2
τfast= 0.5 ms (87 %)
τfast= 1.7 ms (38 %)
τslow= 34 ms (62 %)
τslow= 2 ms (13 %)
50 pA
25 ms

figure 9

A Glycine activation

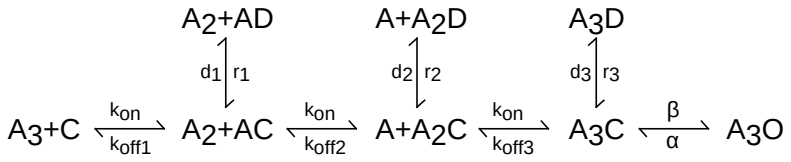

B Picrotoxin inhibition : model 1

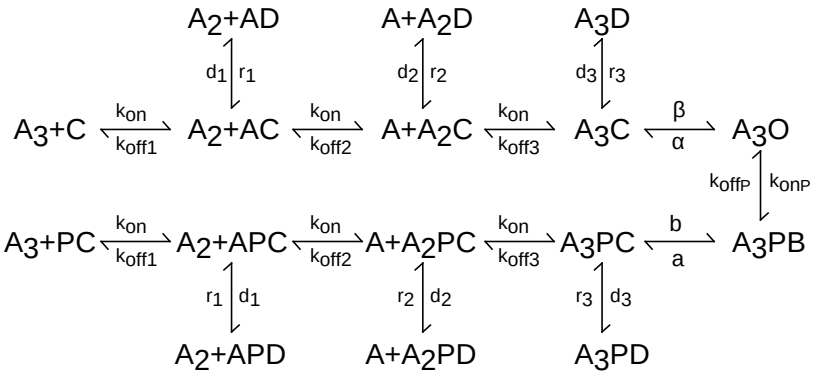

C Picrotoxin inhibition : model 2

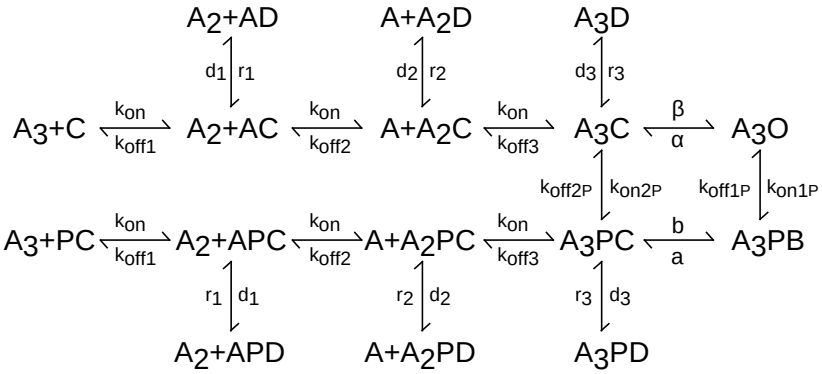

D Picrotoxin inhibition : model 3

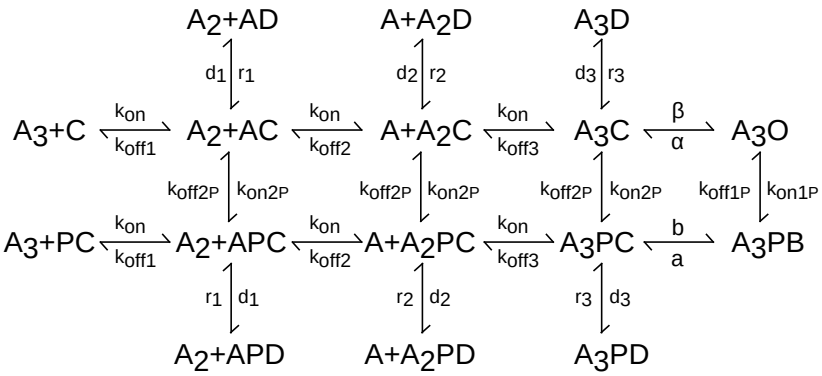

FIGURE 10

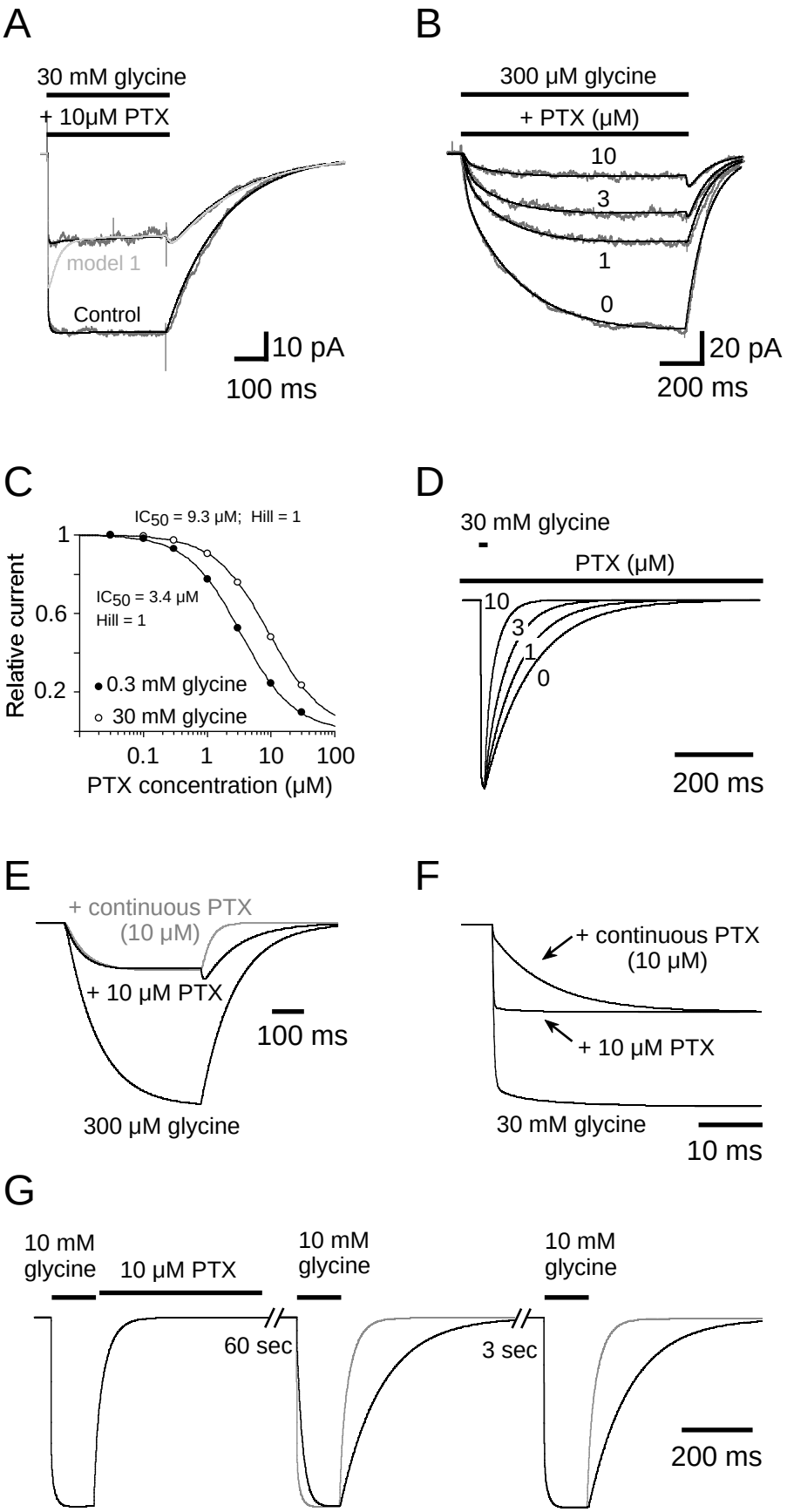
A
30 mM glycine
+ 10μM PTX
model 1
Control
10 pA
100 ms
B
300 μM glycine
+ PTX (μM)
10
3
1
0
20 pA
200 ms
C
IC50 = 9.3 μM; Hill = 1
IC50 = 3.4 μM
Hill = 1
0.3 mM glycine
30 mM glycine
Relative current
1
0.6
0.2
0.1
1
10
100
PTX concentration (μM)
D
30 mM glycine
PTX (μM)
10
3
1
0
200 ms
E
+ continuous PTX
(10 μM)
+ 10 μM PTX
100 ms
300 μM glycine
F
+ continuous PTX
(10 μM)
+ 10 μM PTX
30 mM glycine
10 ms
G
10 mM
glycine
10 μM PTX
60 sec
10 mM
glycine
3 sec
10 mM
glycine
200 ms